Hochschule für Angewandte Wissenschaften Hamburg
Hamburg University of Applied Sciences

Fraunhofer MEVIS

Hochschule für Angewandte Wissenschaften Hamburg
Fakultät Life Sciences

Real Time Tracking of Liver Motion and Deformation in Navigated Liver Surgery by Means of an Electromagnetic System and FEM Simulation

Master Thesis

Biomedical Engineering

Presented by
Dipen Parekh
2055841

HAW Bergedorf, Hamburg
21st April 2013

Supervisor: Prof. Dr. Ing. Thomas Schiemann — HAW Hamburg
Supervisor: Dr. Ing. Darko Ojdanic — Fraunhofer MEVIS

The thesis was supervised and created in Fraunhofer MEVIS Institute

Declaration

I hereby declare and confirm that this master thesis is entirely the result of my own work except where the references are mentioned. All used resources are explicitly referenced in the bibliography.

Bremen, 17th April 2013

Dipen Parekh

Abstract

In this thesis, I present a framework for real time tracking of liver motion and deformation based on FEM by means of an electromagnetic system. The first part of this thesis describes achieving rigid registration between the liver phantom and its MR image by least square estimation of transformational parameters between two point patterns based on ficudial marker mapping. Due to the optimized estimation method the good results are obtained even when the data is corrupted. This transformation matrix obtained enables us to bring all the components in the image space and thus the surgical tool can be localized. This rigid registration can efficiently handle translational and rotational motion.

Second part of the thesis describes the physical simulation and visualization of a liver phantom based on implicit finite element method where the physical simulation is driven by displacement field defined by vector drawn on its 2D image. A non-nested hierarchical tetrahedral volumetric mesh of the liver phantom from is generated and the finite element model of this volumetric mesh is formulated by corotated Cauchy strain. Dirichlet boundary conditions are assigned for surface vertices fixation where deformations are not intended. The marker position is rendered on the volumetric mesh and then the displacement field defined by the vector from marker base alters the finite element model which is solved by a multigrid solver and the mesh geometry is updated.

Both the rigid registration and deformation simulation are then combined into a single system and the deformations are induced by real time external forces defined by displacement field obtained from an electromagnetic tracking sensor attached on the surface on the phantom. This interplay allows for real time visualization of tracking translational and rotation along with deformations performed on the liver phantom.

Table of Contents

List of Figures

Abbreviations

CT	Computed Tomography
FE	Finite Element
FEM	Finite Element Methods
ICP	Iterative Closest Point
IGS	Image guided surgery
LED	Light emitting diode
MR	Magnetic Resonance
MRI	Magnetic Resonance Imaging
OR	Operating room
ROI	Region of Interest
TUM	Technische Universität München
WHO	World Health Organization

1. Introduction

Motivation and Aim

Liver Cancer is a very common disease with poor prognosis. An estimated 750 000 people were diagnosed with liver cancer worldwide in 2008. Globally as of 2008 liver cancer is the third most common cause of death from cancer (700 000 deaths) after lung cancer (1.38 million deaths) and stomach cancer (740 000 deaths) [1]. The ratio of mortality to incidence was 0.92 in 2008. The survival rate for untreated liver metastasis is approximately 12 months, whereas after surgical resection is 28-58% for the overall 5 years. An increase in number of surgical treatments and surgical precision might increase this number and decrease mortality rate and thus leading us towards a potentially curative treatment [2].

In order to proceed for achievement of successful treatment, detailed knowledge of patient-specific vascular and biliary anatomy needs to be combined with sophisticated surgical approaches [2]. Until now, the 3D anatomical data, resection plan, etc. was to be mentally transferred by the surgeon onto the patient in the operating room. No navigation systems were present to guide the surgeon or to localize the tumor precisely, major vessels and vascular territories. This led to development of such navigation systems. Commercial 3D navigation systems are available for bony structures i.e. in neurosurgery and orthopedics. But, there are only a few systems are available which are still in research phase for navigation in soft tissue [3].

Figure 1.1 A General liver surgery without intraoperative assistance [4].

In a general liver surgery, the doctors plan the surgical interventions by analyzing pre-operative images of liver built up either by X-ray computed tomography (CT) or by magnetic resonance imaging (MRI) and by identifying important structures like tumors or resection lines. During the operation, the doctors need to figure out where the tumor and the resection lines are. Such operations are time consuming and need rich experiences. Image-guided surgical techniques could provide this improvement in accuracy over conventional techniques. The most important aspect of IGS is a process called registration. It is basically a mathematical mapping between preoperative images of liver acquired by CT or MRI with intraoperative anatomical presentation of the organ [5]. The other important aspect of IGS is tracking of surgical instruments using a tracking system. The tracking devices are used to track the position of instruments relative to patient anatomy. Optical trackers were developed and then quickly adopted because of their accuracy and large field of view. However, there was a line of sight which was to be maintained between the tracking device and the instrument to be tracked with lead to the development of electromagnetic tracking. Electromagnetic tracking devices have no line of sight requirements and are able to track instruments such as catheters and needles inside the body [6]. With the help of mapping, a real time update of surgical position can be displayed in reference to preoperative images. This mapping does not account for breathing and deformation artifacts. We are ultimately interested in modeling the motion tracking and adaptation of real time deformation into the surgery. One approach is to create a finite element model and assign tissue properties and calculate deformation based on acting forces based on defined landmarks. This method although requires substantial user interaction to identify anatomic landmarks. It is a step forward in modeling deformation of liver.

Real time tracking of liver motion and deformation could be a vital step forward in navigated liver surgery facilitating the surgeon with much needed assistance. This thesis is based on developing an experimental framework which can track the liver motion based on least square modification of Horn's closed form solution using ficudial markers and also adapt deformation based on Implicit FEM simulation developed by Joachim Georgii with help an electromagnetic tracking system on a silicon liver phantom.

2. Navigated Liver Surgery

2.1 Definition

Navigated surgeries are computer based medical procedures that provide virtual image overlays to help the physician precisely visualize and target the surgical site [6]. This requires several pre-requisites to be met, such as an appropriate dataset of the patient, it is properly processed and a virtual 3D model is created, lastly a sufficiently accurate registration procedure. Registration maps the patient with the dataset. Once this is achieved then virtual model of the patient's organ is mapped to the patient. Based on this, surgical instruments are also mapped onto the patient's model and with a help of a tracking system. Such surgeries are characterized as navigated surgeries where there is a direct connection between patient and a virtual model for assistance. Surgical instruments are tracked and thus we can locate them on the patient (with our eyes) and they can also be visualized on the model on the screen (through registration) [7].

Liver surgeries for tumor resections are among the most complex surgical interventions in human body. General liver surgeries follow the following structure.

1. Mark the resection surface.
2. Follow the resection course.
3. Avoid cutting risky structures.
4. Adapt the resection strategy in case of new intra operative findings.

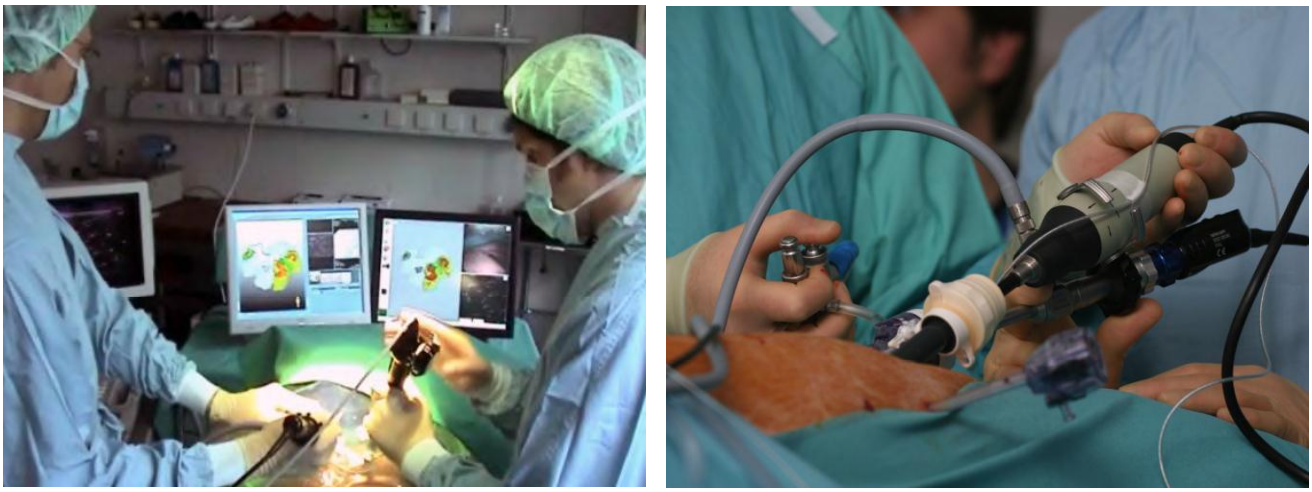

(a) (b)

Figure 2.1: (a): Navigation in liver surgery with tracking tool using a tumor mimic model [8],
(b) Ultrasound based Navigation System for liver surgery using electromagnetic tracking [8]

With the adaptation of navigation into a general liver surgery the additional workflow are included.

1. Preoperative liver images are acquired and a 3D model is generated.
2. Surgical instruments are tracked using tracking device.
3. Intraoperative registration of patient liver is registered to the virtual 3D model.
4. Surgical instruments are displayed relative to the patient liver.
5. Doctor uses this virtual display to manipulate instruments during the surgical procedure.

Navigation support in navigated liver surgery is through intraoperative imaging through registration and continuous tracking of organ motion [8].

2.2 Components

2.2.1 Tracking System

Tracking system are called localizers are an important component of navigation in liver surgery. They have the task of localizing objects in space. Basically they provide us with spatial information about the surgical instruments. There are two types of tracking systems used in modern day navigated liver surgeries [6].

- **Optical tracking systems**

The location of the object is identified by Optical tracking systems by measurement of light transmitted or reflected by the markers provided on them. Optical tracking can be further subdivided into active and passive systems. Systems in which markers emit light typically through LEDs are referred to as active optical tracking systems. Systems in which markers reflect light when illuminated with a light source are referred to as passive optical tracking systems. Active systems are not widely used for medical applications because of their short comings of requirement of cables for running LEDs. Passive tracking is achieved by specific infrared light reflecting markers attached to surgical instruments. The camera captures the reflected light from the markers which was transmitted by an infrared light source.

Optical tracking provides high accuracy and is not influenced by presence of any magnetic fields or ferromagnetic objects nearby. Furthermore, passive tracking does not require any cables hence it does not cause any risk of bacterial infection in the OR. However, the only disadvantage is that it requires a line of sight between the reflected light from markers and the camera. If this line of sight is blocked then the object cannot be tracked. Thus, tracking objects inside the body is not possible. Only surface tracking is possible. Furthermore, any scattered light from a different source can also influence the localization of the object [7].

- **Electromagnetic tracking system**

Electromagnetic systems determine the position of the objects in a pulsed magnetic field. The magnetic field is generated by field generator called transmitter, receivers called sensors are attached to surgical instruments in which voltage is induced by magnetic field. The data is received by field sensors provide an assessment to sensor location. Electromagnetic sensors can be made much smaller than optical markers (0.5 mm in diameter and 8mm in length [8].

(a) (b)

Figure 2.2.1: (a): An Optical Tracking Navigation system from CAScination. ; (b): An Electromagnetic tracking system from Ascension Tech

Major advantage of electromagnetic tracking is that it does not require a line of sight between the transmitter and receiver. Thus, objects can be localized inside the body. However, the sensors require cables which are connected to the tracking system, which increases the chances of bacterial infection and thus decreases the sterility inside the OR. Also, to operate with surgical instruments which have cables attached to them could prove sometime troublesome for the surgeons. Electromagnetic systems are less accurate as compared to optical tracking. Furthermore, electromagnetic tracking suffers two major disadvantages i.e. Presence of another magnetic field can interfere with the field generated by the transmitter and can influence the output of the tracking system. Secondly, objects of ferromagnetic material will also have an influence on the measurements.

Overall, electromagnetic tracking provides reasonable accuracy if there is no interference of the magnetic field by other magnetic fields or ferromagnetic material and has made substantial progress in medical applications [7].

2.2.2 Registration

Registration is an essential component of navigated liver surgery. It is the mathematical mapping which brings the two coordinate systems into spatial alignment. Here, the preoperative images (CT or MRI) are registered with the patient's liver. This process of mathematical mapping can be classified into two types: rigid registration and non-rigid registration.

- Rigid registration

In rigid registration, only translation and rotation of set points on datasets to be mapped is achieved. Deformations are not considered. Rigid registration is mostly 3D-to-3D image registration. Rigid registration does not compensate for translational motion due to respiration and movement artifacts. The registration is stable as long as the liver does not move. Common approach for minimizing these artifacts is intraoperative image acquisition. Intraoperative images are directly used for registration with preoperative data. However, the drawback of this technique is that the surgical procedure has to be interrupted for acquisition of images. Another approach is the placement of ficudial markers on the liver. Thereby the position of the liver is known and thus it can be localized by the tracking device [9].

Minimum number of markers required to compute the transformation are three. However, more markers can be used for optimization of registration errors. Also, the placement of markers will influence the transformation and thus span should be as large as possible. Another disadvantage of rigid registration is that it is only valid as long as there is no movement of liver.

- Non-rigid registration

Here, real time deformation of the organ based on breathing motions and applied external pressure by the surgeon is adapted along with translation and rotation motion is mapped with preoperative data. Currently available non-rigid registration lack robustness required for clinical purposes and has been applied in very limited trials to date [6].

In this thesis, an experimental framework for non-rigid registration is developed based which performs rigid registration based on least square distance minimization of Horn's closed form

solution and deformation simulation based on finite element methods which can handle external forces and real time updates and visualization.

2.2.3 Visualization

Visual information provides approx. 70% of sensory input and obviously important for a surgeon [10]. With the increase of computer assistance and complexity of interventions in surgery, visualization has become an important of liver surgery. Preoperative data can be displayed:

1. Multiplanar reformatting: Data is displayed as a stack of slices which can be scrolled in orthogonal or any arbitrary directions.
2. Surface rendering: Surface are extracted from structures and then displayed as group of polygonal meshes.
3. Volume Rendering: Projection image is produced by computing rays through volumes

3D visualization of preoperative data can be presented as direct volume rendering or surface rendering on a display. Volume rendering is considered as most appropriate visualization technique as it retains all the original data, which has enabled its widespread use in medical image visualization [6]. Volume rendering realizes every voxel of a given organ and define translucidity and reflexivity [10]. Because of its ability to retain all the original data, volume rendering also allows us to see internal structures of the object. Also, for deformation simulation volume rendering is useful to analyze internal material properties directly determined by simulation [11].

During navigated liver surgery, 3D visualization is needed for guiding tracked surgical instruments and rendering deformed meshes of liver. Effective visualizations also provide assistance in resection planning thus increasing confidence and orientation ability of surgeons [8].

3. Technical Framework

Following chapter describes the technological framework used for experimental development during the thesis.

3.1 MeVisLab

MeVisLab was created and developed by Fraunhofer MEVIS (formerly MeVis Research). Since 2008, the development and maintenance of MeVisLab is done as a joint effort between MeVis Medical Solutions and Fraunhofer MEVIS. MeVisLab is platform for image processing research and development with a focus on medical imaging, allowing integration, testing and development of new algorithms for application which can be used in clinical environments [12].

MeVisLab includes advanced medical imaging modules for segmentation, registration, volumetry, and quantitative morphological and functional analysis. It provides flexible 2D/3D visualization and interaction tools, intuitive user interface and a modular, expandable C++ image processing library. Several clinical prototypes have been realized on the basis of MeVisLab, including software assistants for neuro-imaging, dynamic image analysis, surgery planning, and vessel analysis [12].

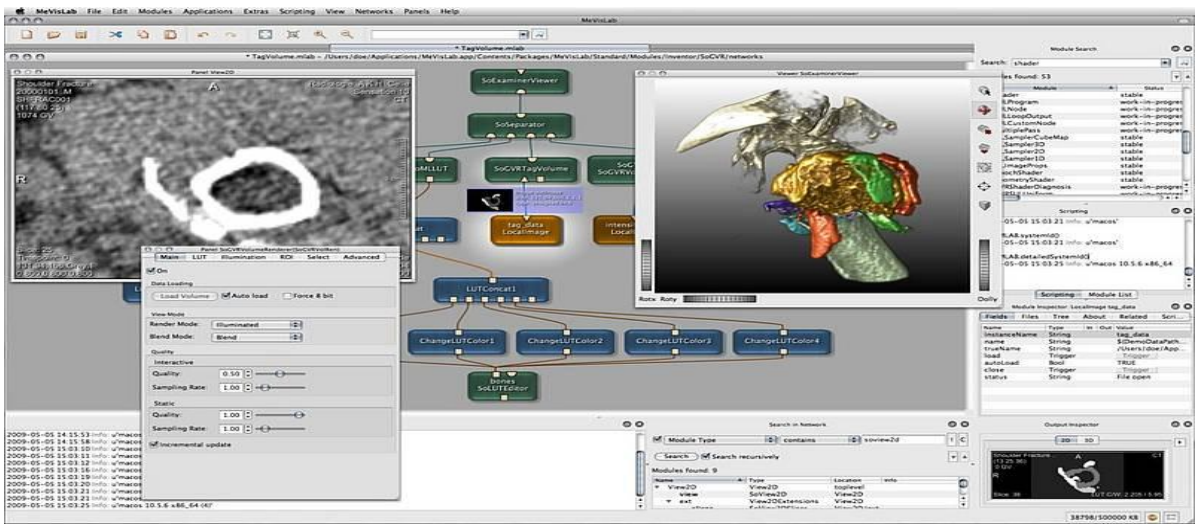

Figure 3.1: MeVisLab framework for image processing and visualization [13]

A fundamental part of MeVisLab is the object-oriented MeVis Image Processing Library (ML) that provides a generic framework for image processing. Each algorithm represents itself as a module which can be used inside the development environment. . More than 300 image processing modules are available. The library also provides unified algorithms for the generation, the processing and the rendering of meshes [13].

3.2 Ascension tracking system

Tracking device used for the development of this thesis is 3D Guidance trakSTAR2© made by Ascension Technology. Ascension Technology makes 3D tracking devices which are used in medical applications such as minimally invasive surgery, real-time visualization and target acquisition.

trakSTAR2© is designed for short range applications. The device is classified as Class I with Type B Applied Parts (Sensors). It is fast and provides dynamic tracking. There is also no inertial drift or optical interference. The device also has immunity for distortion from nonmagnetic metals. trackSTAR2© has two main components: Transmitter and Sensors. Transmitter used is mid-range with transmitting range. Sensors used for this thesis are model 800 and model 130. Both these provide us with 6 degrees of freedom which means position and orientation (6DOF) [14].

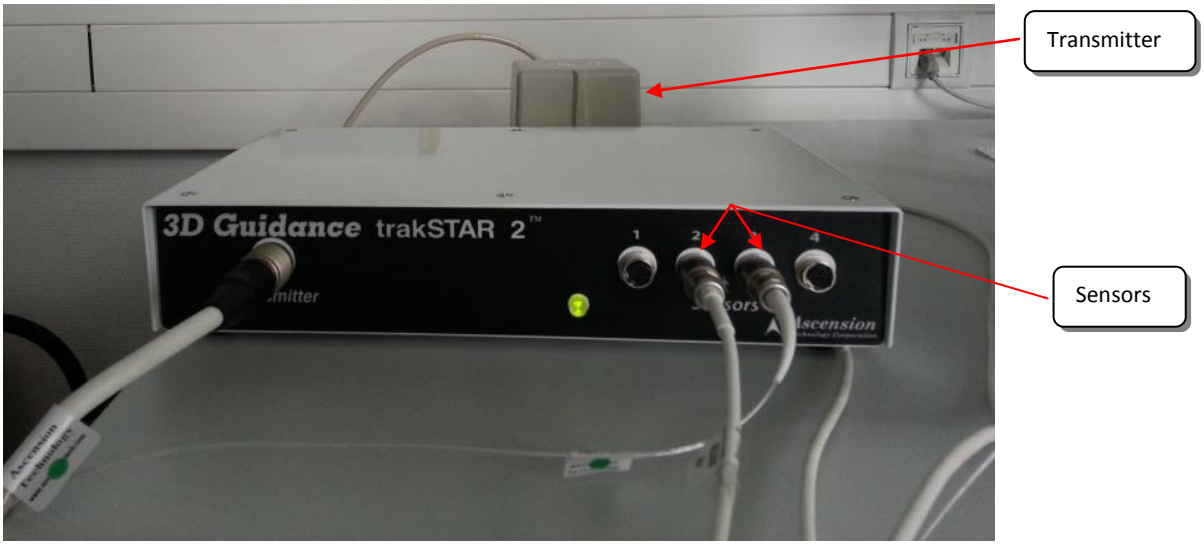

Figure 3.2 Above figure shows the Ascension trackSTAR2 device.

3.3 Silicon Phantom

The liver phantom used for this thesis is made from Ecoflex® Supersoft Silicone 0050 on silicon rubber with red color. Ecoflex® Rubbers are platinum-catalyzed silicones that are versatile. Rubber also cures without a "tacky" surface. Rubber is very soft, very strong and has very good elastic properties. Thus, it is easily deformable [15]. The phantom is attached with 5 MR markers which can be detected in MR image and which are then used as landmarks for registration.

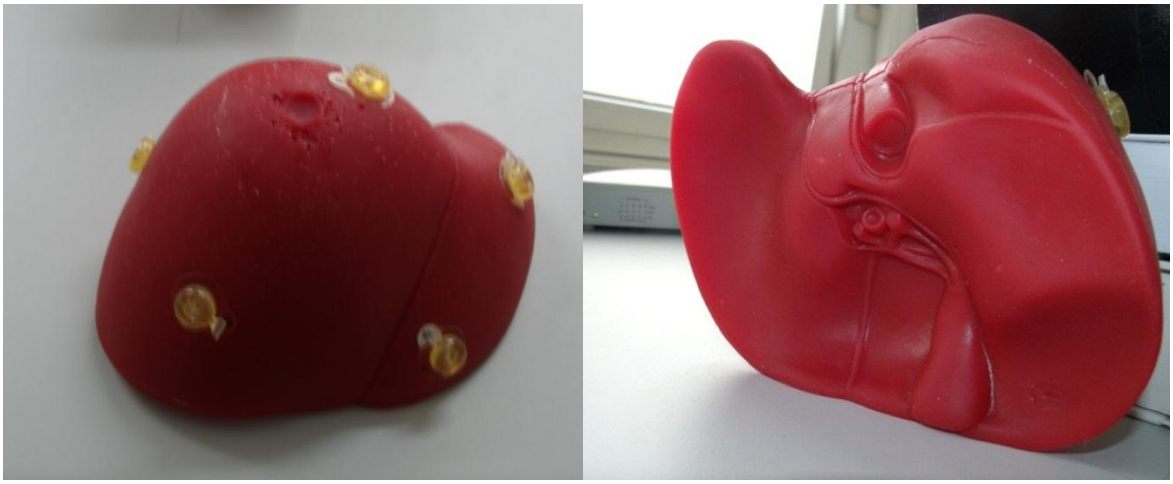

Figure 3.3: Left shows the silicon liver phantom with 5 ficudial markers attached. Right shows the same phantom from the lower surface.

3.4 Deformation Simulation

Deformation simulation used for thesis was presented by Joachim Georgii for his PhD thesis. The framework developed is for physical simulation and visualization of deformable bodies in real time. The framework is based on implicit finite element methods for development of a multigrid approach for numerical simulation of deformable bodies. Approach enables stable simulation of bodies with tetrahedral or hexahedral grids. The simulation technique can deform bodies with varying stiffness. Rendering method was also developed for visualization of deformable bodies, which includes rendering of surfaces as well as interior volumetric structures [11].

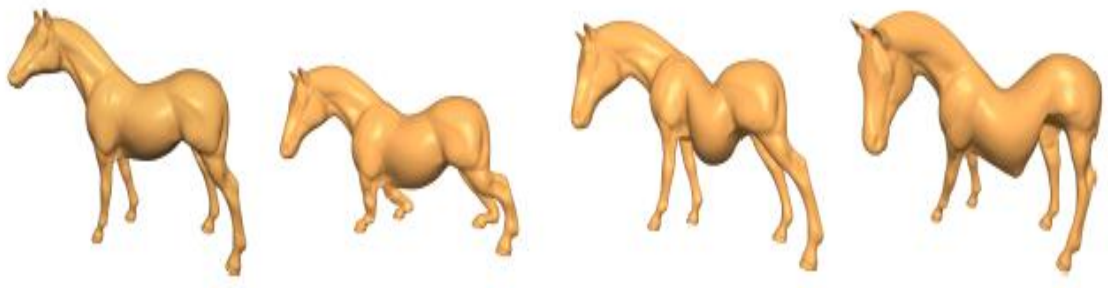

Figure 3.4: The deformation performed on a tetrahedral mesh of a horse is shown. From left to right, the initial model is simulated under different stiffness under gravity and also with external forces using Joachim Georgii's simulation model. [11].

4. Rigid Registration

The following chapter describes the process of rigid registration between the silicon phantom with its 3D model with the help of tracking device using an electromagnetic system. The first step towards rigid registration is registration between the liver phantom and 3D model based on mapping ficudial markers on the liver phantom and on the virtual 3D model. This is done by using least square estimation of transformation parameters between two point patterns. But, this registration is stable only if there is no movement of liver. To track real-time motion of phantom, a sensor is attached to the liver surface. This sensor then facilitates us with the real time localization of the phantom. Now, the registration is achieved with respect to the sensor attached onto the liver phantom. The registration remains stable as long as the position of the sensor on the surface is not altered. Least square estimation algorithm generates a transformation matrix which is then used to localize the surgical tool. The entire process is called rigid registration.

4.1 System Setup

The navigation system is easy to setup. It requires a computer connected with ascension trakSTAR2© device. The surgical tool is also attached with a sensor for localization.

In order to achieve rigid registration, appropriate connections should be established between the 3D model, liver phantom, tracking system and surgical instruments. Registrations must be done to achieve the transformation matrices between these systems.

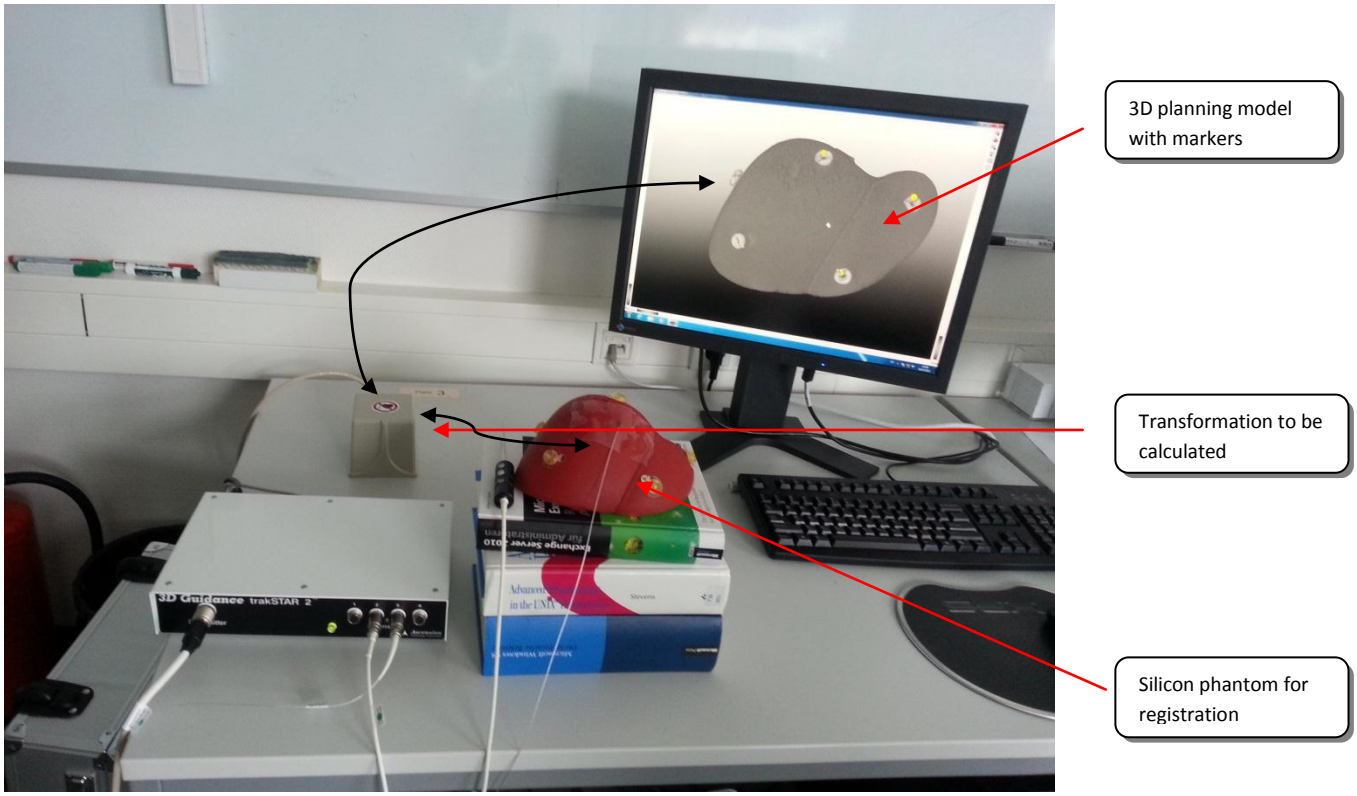

Figure 4.1 System setup for process of rigid registration where the transformation matrix for bringing all variants into one coordinate system has to be calculated.

4.2 Mathematical mapping between the phantom and virtual 3D model

The mathematical mapping between the phantom and the 3D model is based on least-squares estimation of transformation between two point patterns modification by Shinji Umeyama (1991) [16] on closed form solution of absolute orientation proposed by Berthold K. P. Horn (1987) [17]. The methods works on finding the transformation between the sets of same number of points in two Cartesian coordinates systems.

Horn's closed form solution using unit quaternions itself is a robust method for determining the transformation between two coordinate systems, however when the data is severely corrupted the solution fails to give a correct rotation matrix instead provides us with a reflection. The least squares estimation gives us a solution to this problem and it always gives us a correct transformation even when the data is corrupted. The least square estimation method for implementation in used this thesis was already developed and validated at Fraunhofer MEVIS. I have just used the output transformational matrix to bring all the points in one system. This is achieved by formulating the datasets to be mapped and then applying least squares estimation which gives us a transformation.

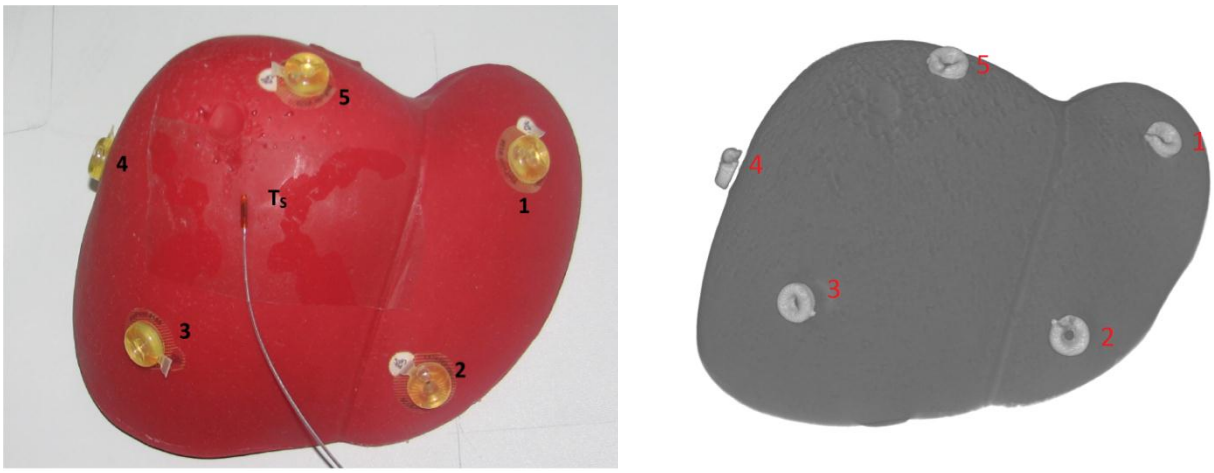

Figure 4.2: Left shows Silicon phantom with sensor attached and numbered markers. Right shows the MR image of phantom with numbered markers

Figure 4.2 shows that the silicon phantom has to be registered with its MR image based on mapping markers in the corresponding order.

4.2.1 Formulation of datasets

The model data, x i.e. the location of the markers on the 3D model comes from the MR image of the phantom by defining the markers interactively in world coordinate system. This completes the formulation of model data.

The collected data, p i.e. corresponding position of the markers on the phantom comes from the surgical tool equipped with a sensor which provides the three dimensional surface information in the coordinate system of the generator.

The location of each marker on the phantom is first known by localizing it with the sensor attached to a surgical tool. The ascension trakSTAR2 localizes the marker in a matrix as $T = \begin{bmatrix} R & t \\ 0\ 0\ 0 & 1 \end{bmatrix}$ where R is a 3 X 3 rotation matrix which indicates the direction of the axis about which rotation takes place plus the angle of rotation about the axis and t is 3 X 1 translation matrix having three degrees of freedom. Now, to achieve the position of the tip from the sensor base, we need to apply a translation offset which provides us with location at the tip. See figure 4.2.1. Transformational matrix for tool tip is given by $T = T_{base}$ X $T_{tip\ offset}$.

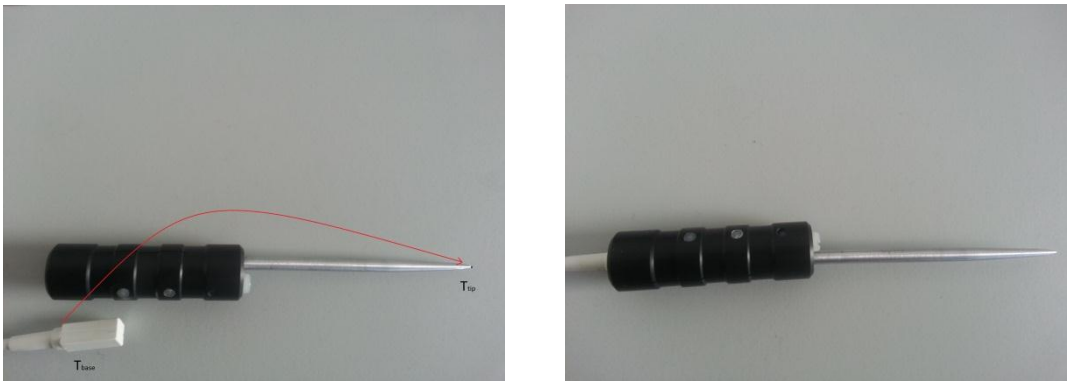

Figure 4.2.1: Left shows calibration tool tip with sensor unattached and right shows calibration tool tip with sensor attached

Here $T_{tip\ offset} = \begin{bmatrix} I & t \\ 0\ 0\ 0 & 1 \end{bmatrix}$, where I is 3 X 3 identity matrix and t is 3 X 1 translational offset, $t = \begin{bmatrix} x \\ y \\ z \end{bmatrix}$ which provides us the distance in mm from the base. For five marker positions, we have five matrices T_1, T_2, T_3, T_4 and T_5. The collected data set has to be

mapped on the model data set using least square estimation modification of Horn's closed form solution of absolute orientation. The transformation between the two coordinate systems can be decomposed into a rotation and a translation component. Translation has three degrees of freedom and rotation has another three and scaling adds one more degrees of freedom. In all we have to determine seven unknowns. So, five points known in each coordinate systems provide us with fifteen constraints (three coordinates each) more than enough to determine these seven unknowns. Least square estimation solution does not require iteration and provides a best possible transformation in a single step. We are just interested in knowing the translational coordinates of these 5 markers because it is enough to calculate the transformational matrix. So, we have now five points M_1, M_2, M_3, M_4 and M_5. This completes the formulation of collected data set p.

4.2.2 Solution Method

Transformation matrix obtained by performing least square estimation is given as

$$\mathbf{T} = \begin{bmatrix} & \text{sR} & & t0 \\ 0 & 0 & 0 & 1 \end{bmatrix}$$

Here, s is a scaling factor; R is a 3 x 3 rotation matrix and $t0$ is a 3 x 1 translation vector between the two coordinate systems. For a given point i in the dataset p and the corresponding point i in the dataset x, the transformation is performed as [18]

$$\mathrm{X_i} = \mathrm{s{\cdot}R}(\mathrm{p_i}) + t0$$

Here, $\mathrm{X_i}$ is a point from a model dataset and $\mathrm{p_i}$ is the corresponding point in the collected dataset which has to be transformed and s is the scaling factor and $t0$ is the translational vector.

As the data is not perfect, there would be a residual error for transformation equation above. As for each point, we won't be able to find for a scale factor, a rotation and a translation. However, an optimized transformation can be found by minimizing the mean squared error by the following function

$$f(s, R, r0) = \frac{1}{5}\sum_{i=1}^{5} \|e_i\|^2$$

Where e_i is defined as:

$$e_i = \mathrm{X_i} - \mathrm{s{\cdot}R}(\mathrm{p_i}) - r0$$

For derivations refer least-squares estimation of transformation between two point patterns modification by Shinji Umeyama [16] the optimized R, s and $r0$ are determined which gives us the transformational matrix which maps the collected data onto the model data and thus combining the two coordinate systems.

4.2.3 Evaluation of Solution Method

In this section one testing result using the least square estimation is demonstrated using a set of five moving points with five fixed points.

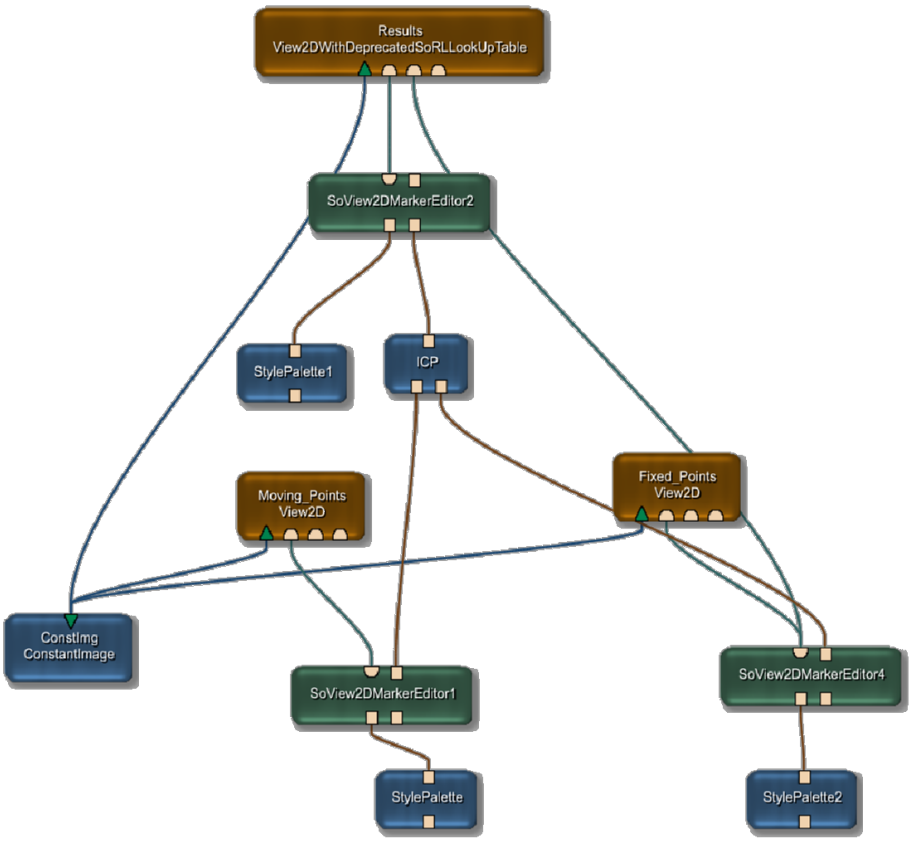

Figure 4.2.3.1: MeVisLab framework for least square estimation of transformation and its visualization

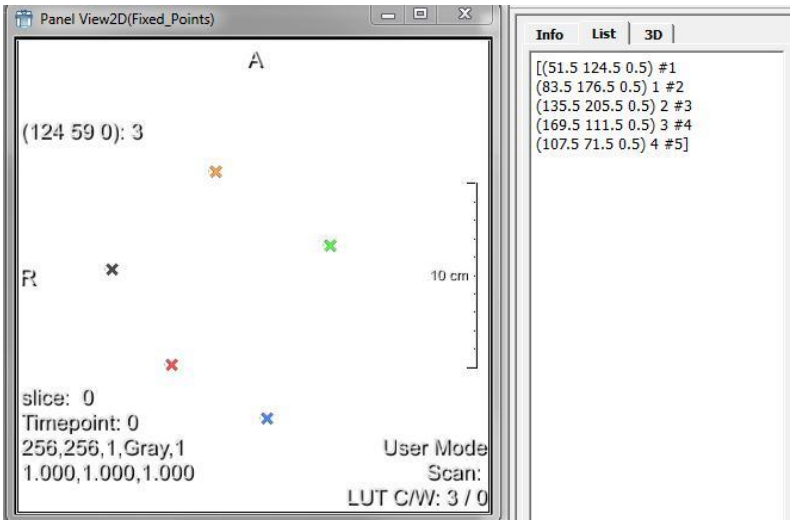

(a)

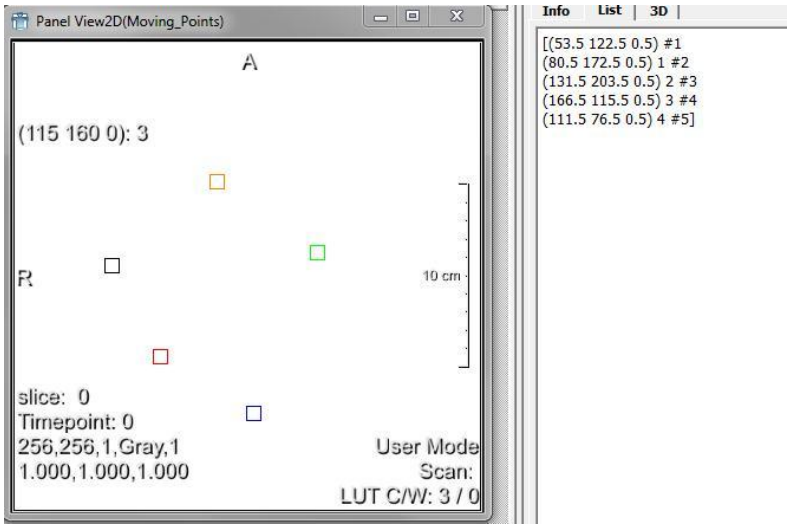

(b)

Figure 4.2.3.2: (a): panel showing 5 fixed points; (b): panel showing five moving points

A small MeVisLab framework was made for evaluation of solution method (see Figure 4.2.3.1). 5 points were fixed in one coordinate system which are given input as right input markers (see Figure 4.2.3.2a) and 5 points were drawn arbitrarily but in congruence to the fixed points which are inputted as left markers(see Figure 4.2.3.2b).Absolute Orientation with least square modification was performed and a transformational matrix is obtained (see Figure 4.2.3.4). Transformed points are shown as output markers (see Figure 4.2.3.3).

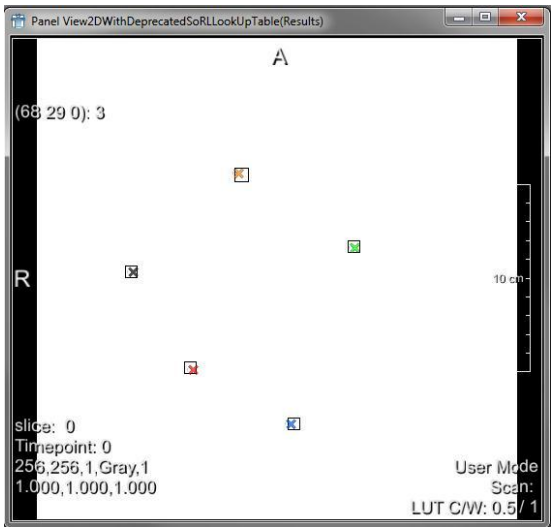

Figure 4.2.3.3: Panel shows output of transformation

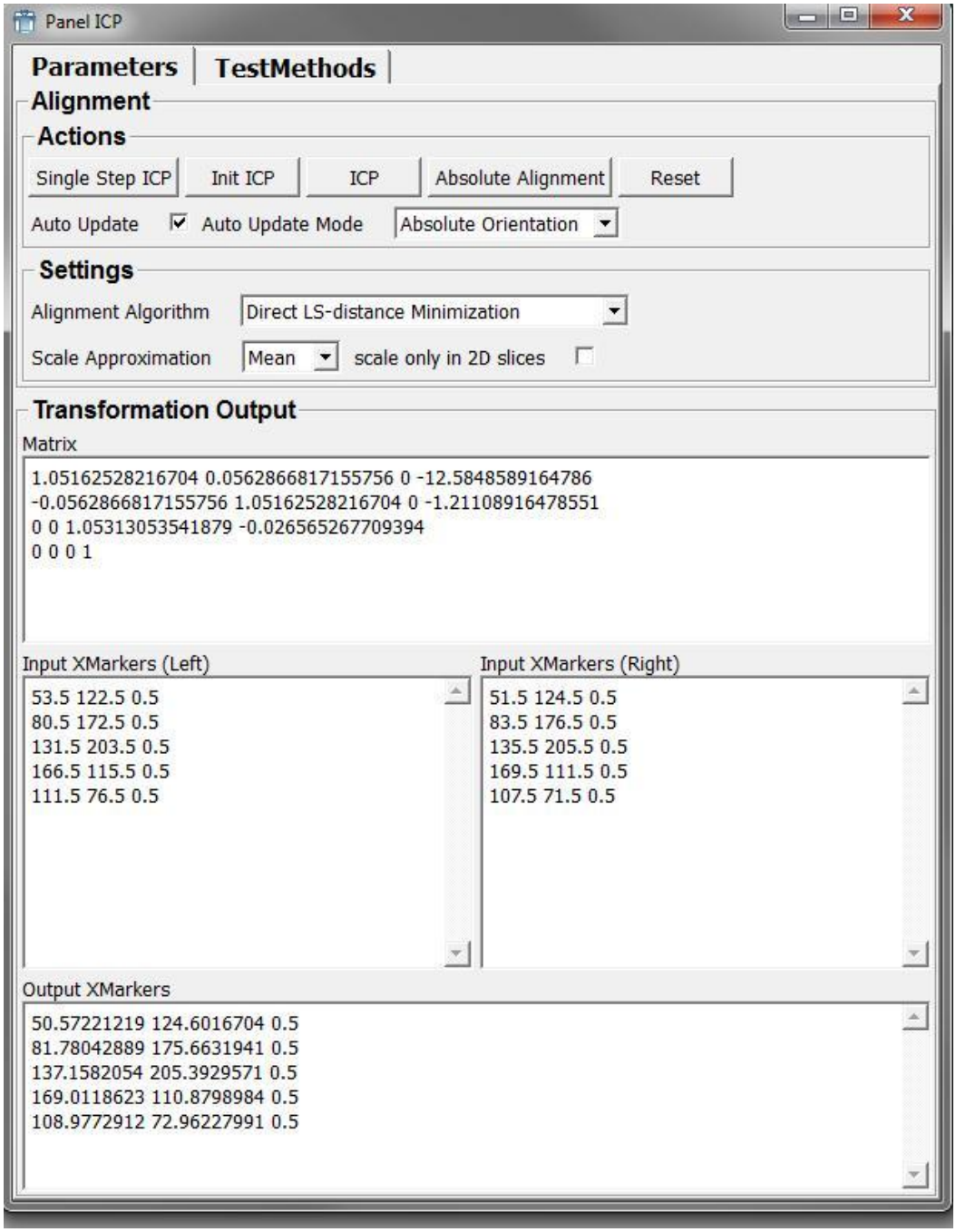

Figure 4.2.3.4: ICP panel which provides us with least square estimation of transformation parameters between two point patterns.

From Figure 4.2.3.4, it is seen that the error between fixed markers (right markers) and the transformed markers (output markers) is not that substantial and is acceptable.

4.3 Real time registration and localization of surgical instruments

4.3.1 Real time registration

The initial registration is achieved based on localizing the markers with help of surgical tool. This registration is stable until the phantom moves. In order to achieve real time registration we need to localize each marker based on the sensor attached to the phantom. So, we need to modify the collected data set with new marker positions with respect to the sensor. Now, the sensor attached to the surface of the liver phantom is also providing us with its location in a matrix with $T_S = \begin{bmatrix} & Rs & & ts \\ 0 & 0 & 0 & 1 \end{bmatrix}$.

The formulation of the data set is achieved by $Ms_i = T_S \times [(T_S)^{-1} X\ M_i]$.

Where, Ms_i is the position of i^{th} marker with respect to sensor in the coordinate system of generator.

Here, to achieve real time location of the markers. $[(T_S)^{-1} X\ M_i]$ is done just once and this multiplication gives us five new points, which are then are again configured with respect to T_S. The multiplication with T_S is done continuously which results continuous formulation of collected dataset ƿ.

This is done in order to shift the localization of ficudial markers to the sensor attached onto the phantom. The transformation matrix is constantly calculated based on the localization of the attached sensor i.e. if the phantom is moved, then T_S which is the matrix for sensor attached to the phantom also changes, but the alignment of the ficudial markers with respect to the sensor is not altered. These markers are now localized with reference to the electromagnetic system. Now, collected data for least square estimation is calculated corresponding to the movement of the phantom, we achieve a constantly updated transformational matrix. This transformation matrix is applied for visualization of liver. This constantly updated transformation matrix calculated using then used for localization of surgical instruments. This registration is valid as long as we do not change the position of the sensor on the phantom.

4.3.2 Localization of surgical instruments

A sensor is attached to the surgical tool which helps in localizing its position. This localization is given as T_{base} and T_{tip}. These are transformation matrices of base and tip. Localization of surgical instrument is achieved as

$$\mathbf{T}_{lb} = \mathbf{T} \times T_b$$

$$\mathbf{T}_{lt} = \mathbf{T} \times T_t$$

Thus, the surgical tool is also localized in the same coordinate system and is applied for visualization of liver. Now, we have everything in the coordinate system of MR image.

This completes rigid registration framework where, silicon phantom is mapped with its 3D model with the help of tracking device using an electromagnetic system. Also, the surgical instrument is localized in the same frame.

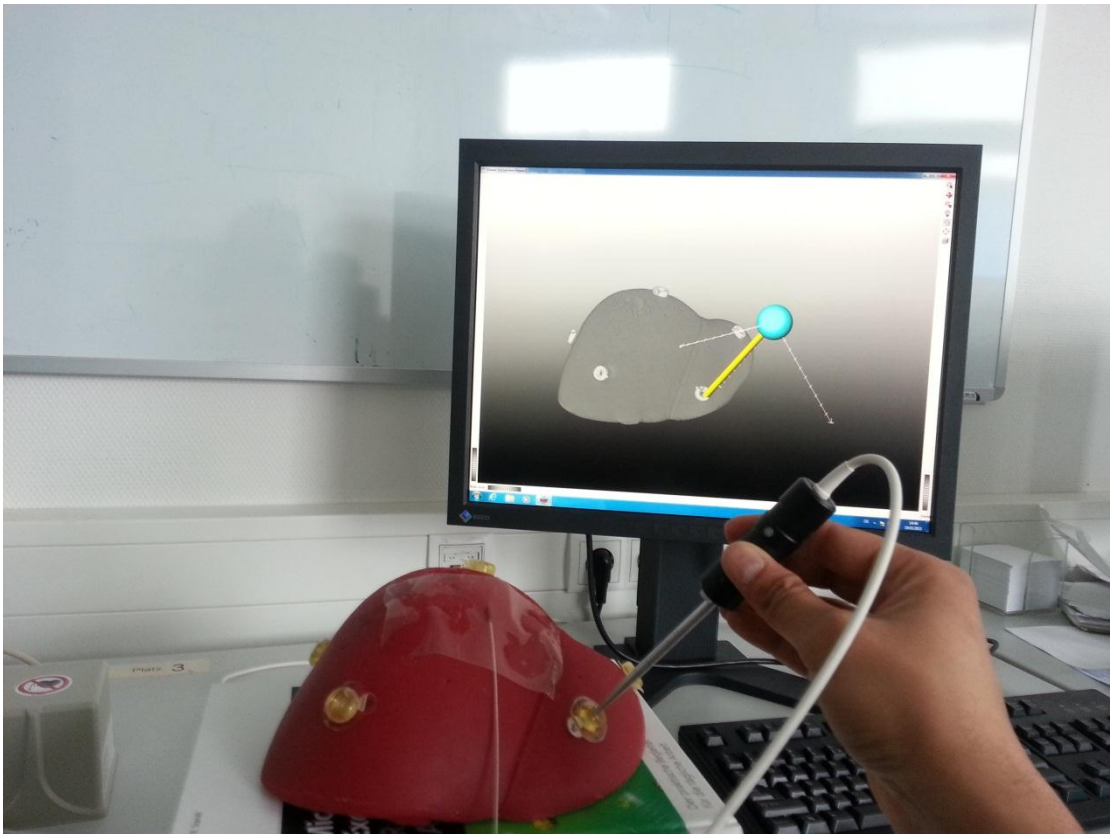

Figure 4.3.2.1: Above figure shows the localization of the surgical tool in the world coordinate system of the MR image.

5. Real time deformation and visualization of liver phantom based on external forces

In this chapter we address a specific issue of deformable bodies i.e. modeling liver deformation with real-time constraints based on finite element method and on techniques to simulate highly resolved meshes which are generated from MR images. Deformation Simulation based on FEM was developed by Joachim Georgii [11]. In this thesis we focus on defining boundary conditions for liver that can fixate a mesh surface and then visualize the deformation in real time.

5.1 Introduction

Fast and reliable deformation simulation methods for 3D bodies is of major importance in medical applications mainly for non-rigid registration, mainly due to correction which needs to be applied for breathing and motion artifacts generated during surgical intervention to ensure desired outcome. Preoperative CT/MR images are to be deformed and registered to support the surgeon in navigation. Important aspect of applying deformation simulation in surgical interventions is the efficiency or real time fast feedback. Robustness of simulation methods is also required, especially if the simulation is patient specific based on individual models.

Finite element methods are best known techniques to accurately model the behavior of deformable objects based on theory of elasticity and thus they are state of art technique for physics based simulation [11]. 3D finite element analysis has been performed in a number of approaches to predict the mechanical response of deformable materials. FE methods are attractive because models are well understood which makes it possible to realistically predict mechanical response of such materials [19]. The deformation simulation developed by Joachim Georgii is used for this thesis is adaptable for real time environments.

FEM simulation model works in following order:

1. Load an image to create a model
2. Select the geometry from deformation package
3. Mesh the model
4. Apply initial and boundary conditions (constraints and load) on the mesh model

5. Solve numerical equations
6. Visualize the results

Here, steps 1 to 4 are considered as preprocessing whereas step 5 is processor and step 6 is post processing. The most difficult and time consuming steps of FEM simulation is preprocessing part where we need to create a finite element model. This step includes generation of mesh and applying correct loads and boundary conditions. It is very difficult to apply boundary conditions that correspond to a real situation. FEM solvers in step 5 i.e. multigrid solvers work automatically but are computationally intensive. Powerful visualization tools can allow real time update of deformation in step 6. The following chapters will provide detailed explanation of these steps.

FE methods are computationally intensive as they require solving a large system of equations. A way to overcome this problem is to analyze the mechanical properties of a deformable body beforehand and based on this information number of finite elements of a model can be reduced preserving simulation accuracy. This is explained in the section of initial conditions. Another way is by choosing low resolution models in combination with high resolution surfaces for rendering purposes reduce the computation cost. This is shown in the section of Volume Mesh generation.

5.2 Volume Mesh Generation

Simulations to be carried out using FEM consist of discretization of a displacement field at a set of points onto the determined model into different structural elements connected with nodes. This group of nodes and elements form the mesh of finite element model. Depending on the model to be simulated, different element types can be used to construct a mesh. An element of the mesh is defined by its geometry: triangle, quadrangle, tetrahedron… In 3D case, where we want to conserve all the voxel morphology and to perform a more efficient stress analysis, volume mesh needs to be constructed. Volume meshes are usually composed of solid element such as tetrahedrons and hexahedron (see Figure 5.2.1). These model structures can be put into different physical conditions such as forces, temperature and pressures in order to see the mechanical responses using finite element analysis [20].

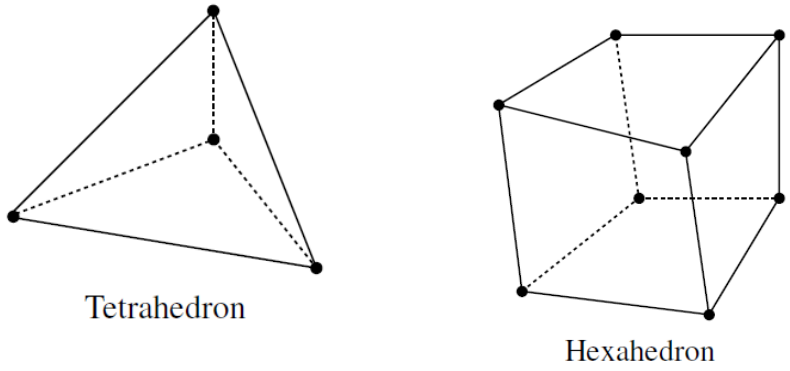

Figure 5.2.1: Left shows 4-noded tetrahedron used in Finite Element volume mesh and right shows 8-noded tetrahedron used in Finite Element volume mesh [11].

For this thesis, a tetrahedral volume mesh was constructed using volume mesh generation package developed by Joachim Georgii at TUM. Figure 5.2.2 shows a MeVisLab network for volume mesh generation.

The motivation for using tetrahedral mesh over hexahedral mesh comes from a geometric point of view. Meshing anatomical structures such as liver which has curved and circumvoluted parts with hexahedral is a difficult part. To obtain a smooth surface a large number of hexahedrons are required whereas comparatively a smaller number of tetrahedral would just be adequate [21]. Also, a hexahedral mesh has 8 DOF compared to tetrahedral which has 4 DOF, which also makes computationally intensive to solve.

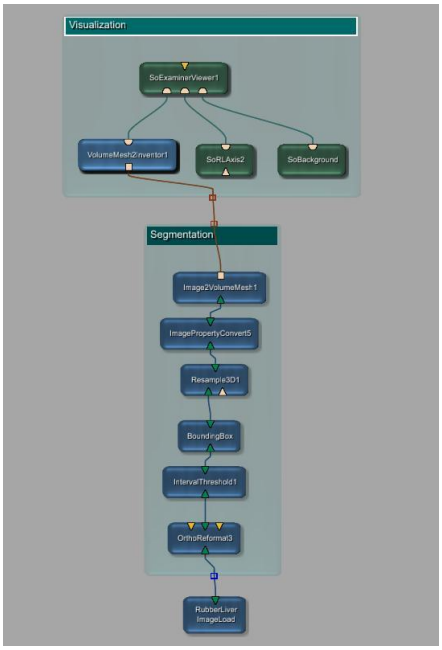

Figure 5.2.2: MeVisLab framework for volume mesh generation

Mesh hierarchy that represents the deformable object at different levels of resolution is required by the multigrid solver developed for simulation (Multigrid solver is explained in section 5.5.2 in this thesis). On this hierarchy, mapping of quantities between different levels using appropriate operators is done. A common way to construct a hierarchy is a top-bottom approach where the tetrahedral is split as shown in Figure 5.2.3. This results in nested hierarchy but it requires the initial mesh to be fine enough to achieve proper representation of object's boundary. Also, these divisions lead to a fine mesh which contain ill-shaped tetrahedral that are not suited for finite element simulation [22]. To overcome these disadvantages, linear operators which establish relations in a multilevel hierarchy of unstructured and unrelated meshes are used which can be efficiently integrated into the multigrid scheme (see Figure 5.2.3). For this, we use barycentric interpolation to map values from a coarse mesh into a fine mesh. Image on the right in Figure 5.2.3 illustrates geometric relations between elements in non-nested hierarchy, shown in 2D. Here grey and black lines indicate coarse mesh and fine mesh respectively. Barycentric interpolation weights are highlighted by red lines [22]. Multigrid method computes the correct FEM solution which avoids inconsistent deformation at different hierarchical levels. Using this network shown in Figure 5.2.2 a hierarchical tetrahedral mesh of the silicon phantom from its MR image is generated. Figure 5.2.4a and Figure 5.2.4b show the constructed volume mesh from the MR image.

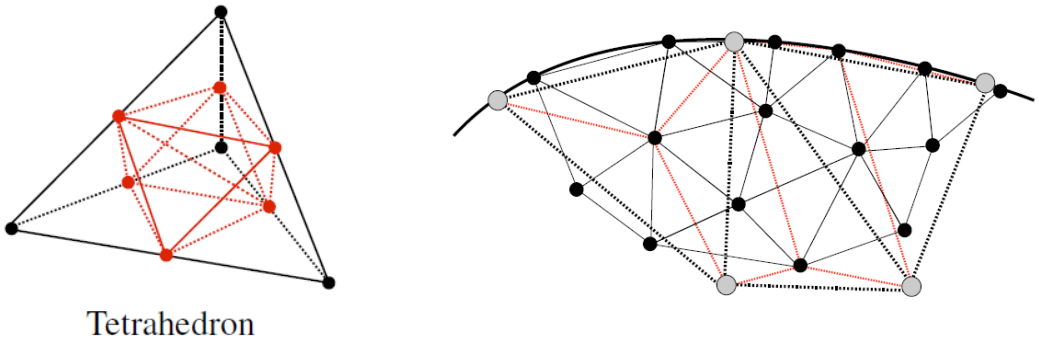

Figure 5.2.3: Left shows a regular division scheme for 4-noded tetrahedral. New vertices are shown in red and new edges are highlighted in red and right shows geometric relations between elements in a non-nested hierarchy are illustrated, a 2D case is shown for simplicity [11].

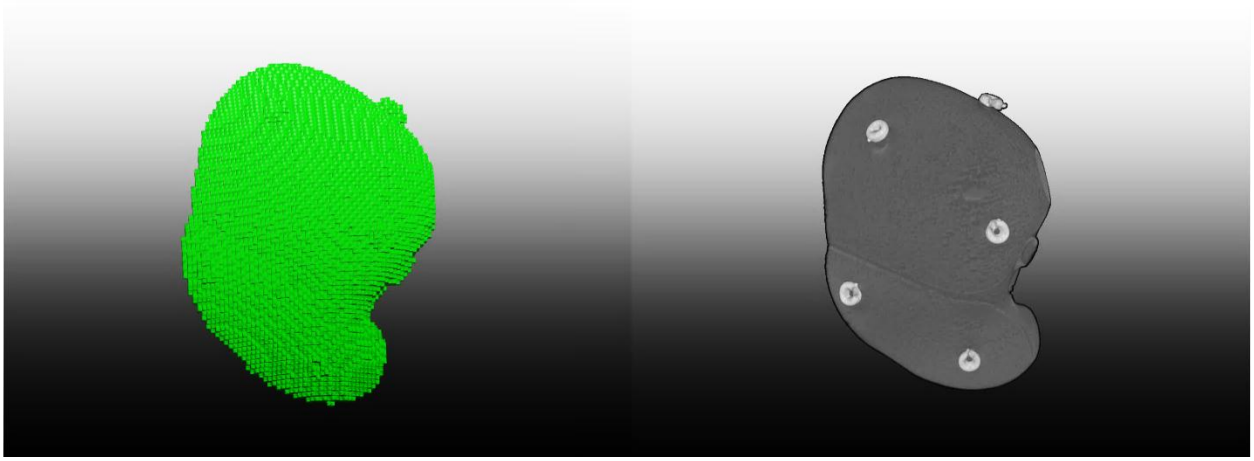

(a)

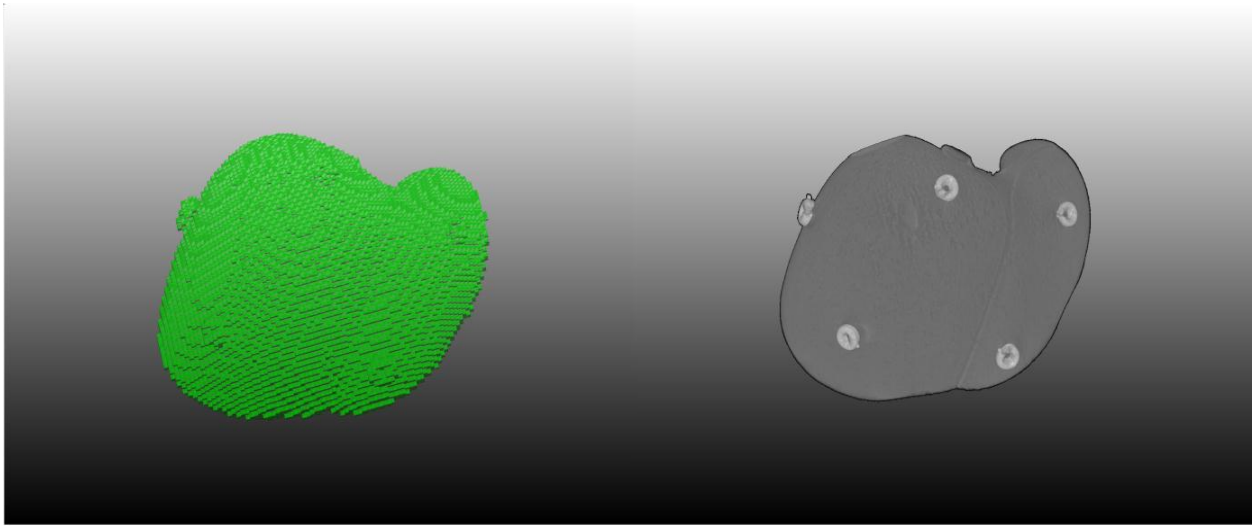

(b)

Figure 5.2.4(a): Left shows coronal view of a hierarchical tetrahedral volume mesh of the MR image and right coronal view of the MR image of the silicon phantom. ; (b): Left shows top view of a hierarchical tetrahedral volume mesh of the MR image and right shows top view of the MR image of the silicon phantom

Finite element models are computationally intensive to solve and to adapt them into real time simulations we choose low resolution models in combination with high resolution surfaces for rendering purposes which in a way reduces the computation cost. For this, we resample the original MR image with a scale factor of .3333 keeping the voxel size constant. Thus, we have a low resolution MR image which is then used for hierarchical tetrahedral mesh generation. The volume mesh shown in Figure 5.2.4a and Figure 5.2.4b has three scales of resolution which assists the multigrid solver to solve the finite element model. The tetrahedral mesh has following configuration.

Level 0: 60045 elements; 68415 vertices

Level 1: 8526 elements; 10716 vertices

Level 2: 1330 elements; 1939 vertices

5.3 Initial Conditions

FE methods are computationally intensive as they require solving a large system of linear equations. A way to overcome this problem is to analyze the mechanical properties of a deformable body beforehand and based on this information number of finite elements of a model can be reduced preserving simulation accuracy.

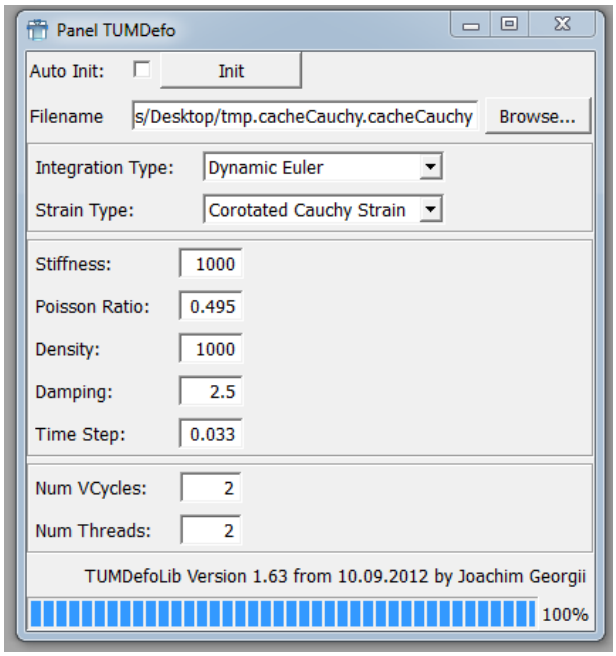

Figure 5.3.1: MeVisLab panel for Deformation simulation where mechanical properties can be predefined.

The strain formulation influences the behavior of the elements under stress. Cauchy strain is linear and hence fast, but only appropriate for small deformations which is just enough for the experimentation of this thesis. The time integration step used is Dynamic Euler. For more information regarding strain formulation and time integration please refer Joachim Georgii's PhD thesis [11]. Stiffness (N/m^2) (elastic modulus) defines how much an element deforms under given forces. A good starting guess for solid materials is 10^6 whereas for very soft (e.g. fatty) tissue can be in the order of $1*10^3$ to $3*10^3$. For Silicon rubber we have chosen elastic modulus of 1000. Poisson ratio of the tissue defines how much the tissue expands orthogonal to the pressure direction. Range is between -1 and 0.5, where 0.5 is a material that maximally spreads out under pressure (like gum) while it preserves its volume, and 0 will do this the least (like cork, for example) while the volume may be reduced. Density of the material, water has 1000 [kg/ m^3], and this is a good assumption for most body tissues. Damping

factor used is 2.5. All this and plus node and element information for analysis and simulation is stored into a simulation cache file. Figure 5.3.1 shows the panel for defining initial conditions and mechanical properties which have been defined for simulation of silicon phantom.

5.4 Finite Element Approaches and Multigrid Solver

5.4.1 Finite Element Approach

For the dynamic behavior of a deformable object to be simulated, we need to derive equations which map the solid's reference configuration $\Omega \subset R^3$ using a displacement function $u(x)$, u: $\Omega \rightarrow R^3$ to its deformed configuration $\{ x + u(x) | x \in \Omega \}$. The displacement function describes the displacement vector of every point $x \in \Omega$. The dynamic behavior of an object with linear elastic response is governed by Lagrangian equation of motion

$$M\ddot{u}+C\dot{u}+Ku = f$$

where M, C and K denote the mass, damping and stiffness matrices respectively [19].Here, u is a vector containing all the displacement vectors of all the vertices and f contains the pre-vertex force vectors. By discretization of u, $\dot{u}$ and $\ddot{u}$ with respect to time, differential equations are transformed into set of difference equations. A second order accurate Newmark scheme is implemented for time integration [22]. When a finite element method is used for modeling a system, the system matrices M, C and K are built from the element matrices derived from the mesh. Since each element has a very small number of neighbors, this FEM system is very sparse. Matrices M and C are derived from simple mass lumping and Rayleigh damping respectively. Stiffness matrix K depends on the elastic energy stored in the solid and on the work done by forces and displacements field u and thus it accounts for the strain energy in congruence with displacement field.

A thorough derivation of equations concerning linear elasticity can be found in the literature [23]. For this thesis, a formulation which is a good trade-off between Cauchy linear strain and non-linear Green strain tensor called corotated strain tensor is used. Because, Cauchy strain suffers from a problem of becoming a variant under rotations, especially if large deformations are applied, it tends to produce artificial forces yielding unwanted results (see Figure 5.4.1 and Figure 5.4.2). Whereas on the other side non-linear strain increases computational complexity as it requires to solve a large system of non-linear equations. Non-linear approach using Green strain tensor also suffers from another disadvantage that the whole system of non-linear equations with all the polynomials has to be stored in memory [11], making it very difficult to adapt for real time simulations as it would be computationally very expensive.

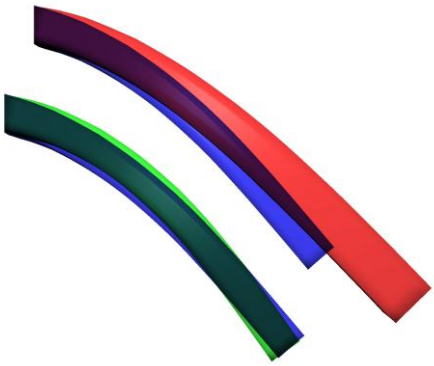

Figure 5.4.1: Comparison of linear (red), corotational (green) and non-linear (blue) simulation. While, Cauchy strain tensor fails to approximate the deformation properly, only very small differences can be observed in case of corotational strain with non-linear strain formulation [11].

Rotational invariant formulation of the Cauchy strain is obtained by corotated formulation by splitting the motion of every element into a rigid body motion with respect to element's initial configuration. Basically, deformed finite elements are first rotated into a configuration that matches the best reference configuration hence, rigid body motions of the element are eliminated before Cauchy strain is computed [19]. So, here the strain is still approximated linearly, artificial forces which are computed using Cauchy strain is significantly reduced. Once the rotation of all elements is calculated, stiffness matrix is reassembled. The solution to the Lagrangian equation of motion is then found by solving a system of linear equations with the updated system matrix K [22].

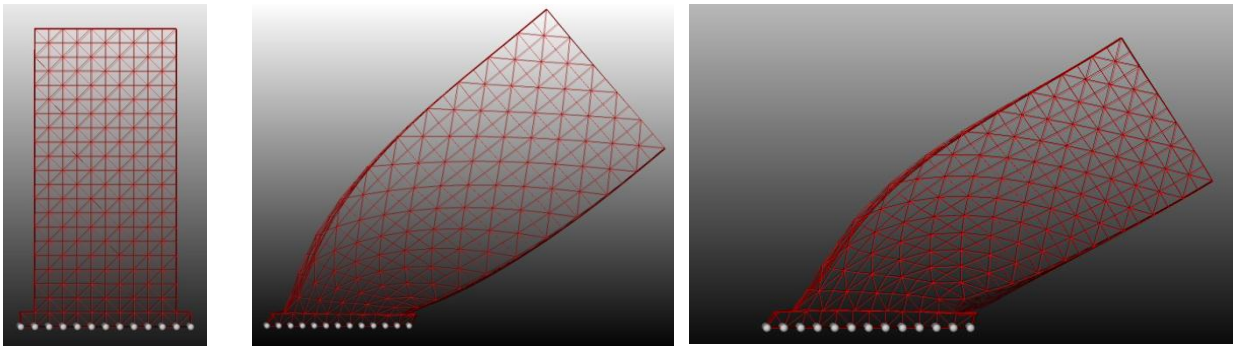

Figure 5.4.2: From left to right a 3D hierarchical tetrahedral mesh of a tower with bottom surface fixed on which deformation will be applied and result of deformation based on gravity with linear Cauchy formulation and corotational formulation strain.

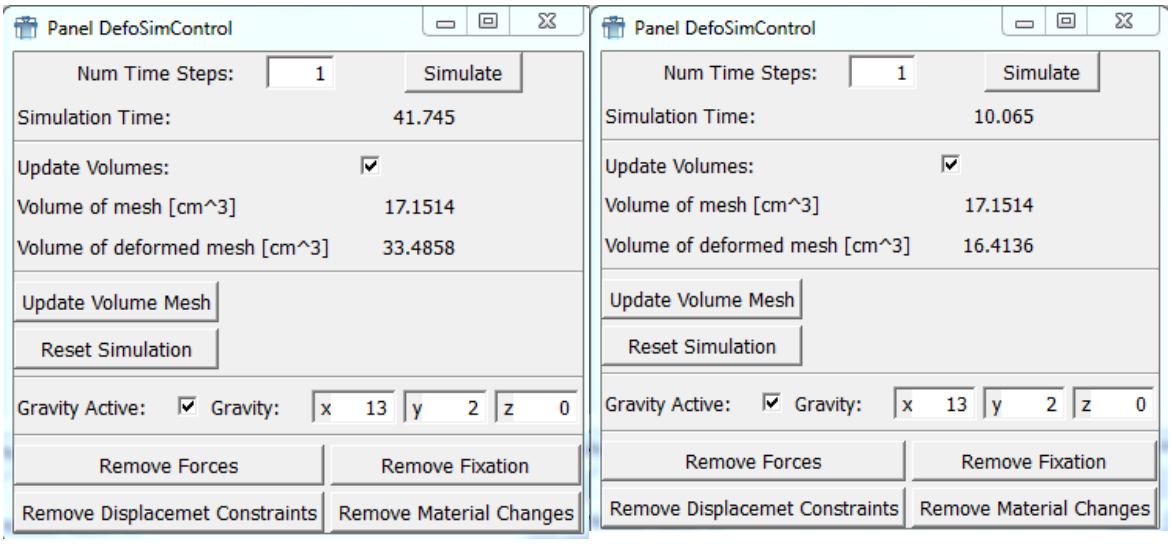

Figure 5.4.3: Left shows the gravity forces applied with linear Cauchy Formulation on the tower and Right shows the gravity forces applied with Corotated formulation. Cauchy strain tensor fails to approximate the deformation properly when large forces are applied; it induces false forces on the elements and thus giving incorrect results. This can be easily seen from the volume of deformed mesh using Cauchy strain as compared to Corotated strain.

Based on the above results and for modeling of silicon phantom deformation on which external forces will be applied and deformation simulation model has to be adapted into real time, corotational formulation of strain is a better choice as compared to linear Cauchy strain. This corotational formulation basically neglects the quadratic terms in the strain tensor, yielding a linearized strain tensor. But this is performed after the elements are rotated into their original configuration. This results in a system of linear equations, just that the system matrix is constantly updated. This system of equations is then solved by multigrid solver.

5.4.2 Multigrid Solver

A numerical solver used for solving the system of equations has to take following into account.

1. The matrices derived using FE meshes are scattered sparse and thus efficient data structures for these matrices are required in solution process.
2. The stiffness matrix is constantly updated. Thus, data structures to efficiently support matrix updates are required.

These two properties are effectively taken care by multigrid framework developed by Joachim Georgii. A basic property of iterative solvers for a system of linear or non-linear equations is that they reduce the high frequencies in the error very quickly while low frequencies are reduced slowly known as smoothing. These low frequency errors can be solved on a coarser grid. A multigrid strategy combines both observations. Multigrid framework is very efficient and accurate because only smoothed error is transferred to the coarser grid. Basically, multigrid solvers exploit the fact that a problem can be solved on different levels of resolution [11].

For efficient and accurate simulation of deformable objects, geometric multigrid method is used. This method includes geometry-specific relaxation, restriction and interpolation operators. These operators form the essential multigrid components, as they are used to transfer quantities along the object hierarchy. That is the reason why we have a hierarchical tetrahedral volume mesh for computing finite elements developed as explained in section 5.2. A thorough explanation of implicit multigrid solver can be found in the literature [11]

5.5 Boundary Conditions

For the purpose of achieving object deformation, it is essential that particular mesh vertices or even regions should be fixed in order to restrict the effects of applied forces. Deformation simulation in medical application consists of modeling parts which include soft tissue or bone structures, thus defining boundary conditions is one of the most important aspect of deformable bodies simulation in medical applications. This is achieved by zeroing all the entries for a vertex to be fixed and by setting the respective vertex force to zero or by associating a constant force to it [11]. There are different approaches to set boundary conditions. Soft bound boundary conditions are defined stiff springs which connect a node with a fixed point [24]. Hard bound boundary conditions are Dirichlet conditions that pre-define the position of selected vertices. Using Dirichlet conditions modify the system of equations for boundary vertices as well as adjacent vertices [19].

Having already obtained Global stiffness matrix, the displacement equations are given as below. Let the subscript f denote fixed displacements and a denote active displacement. The system of linear equations can be defined as

$$\begin{pmatrix} K_{ff} & K_{fa} \\ K_{af} & K_{aa} \end{pmatrix} \begin{pmatrix} U_f \\ U_a \end{pmatrix} = \begin{pmatrix} F_f \\ F_a \end{pmatrix}$$

where the values of displacements U_f are known and applied external forces F_a are also known. The unknown forces F_f and active displacement field U_a are determined as

Solve for U_a: $K_{aa}U_a = F_a - K_{af}U_f$

Compute F_a: $F_a = K_{ff}U_f + K_{fa}U_a$

The solution process is restricted to sub block K_{aa} of matrix, as the system matrix can be updated by setting respective entries to zero. This basically means that for a number of vertices for which displacement is known and the other vertices are fixed by setting their forces to zero, a deformation configuration is obtained that matches the displacement and the other parts of the object are deformed with respect to its physical model [11].

Assigning boundary conditions to the tetrahedral mesh, fixation of vertices of particular region from an input mask image based on Dirichlet conditions is used. Different regions of the liver then have to be segmented in order to obtain a mask which can be used for fixation.

Also, these regions have to be defined pre-operative. For this thesis, the lower surface is considered to be fixed. So, an image processing framework was developed to generate a mask (see Figure 5.5.1) of a lower surface. This, mask is then applied onto the tetrahedral mesh (see Figure 5.5.2). Now, all the surface vertices covered by the mask are fixed.

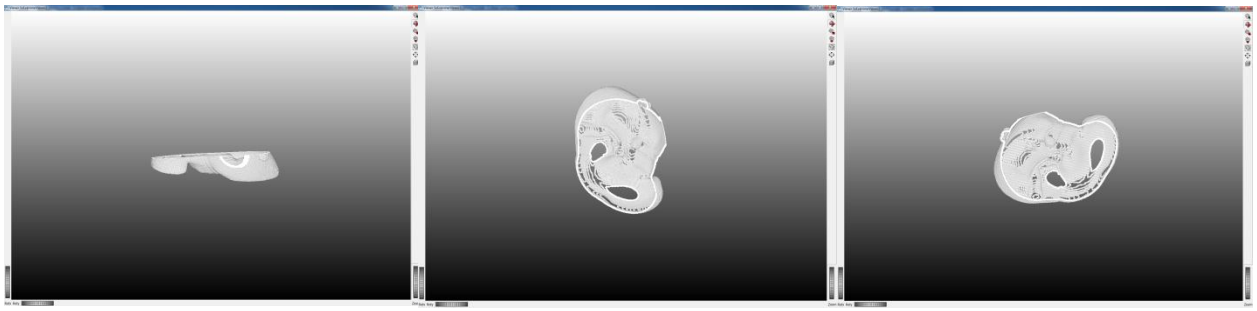

Figure 5.5.1: Left to Right shows the mask for the lower surface generated for fixation of surface vertices.

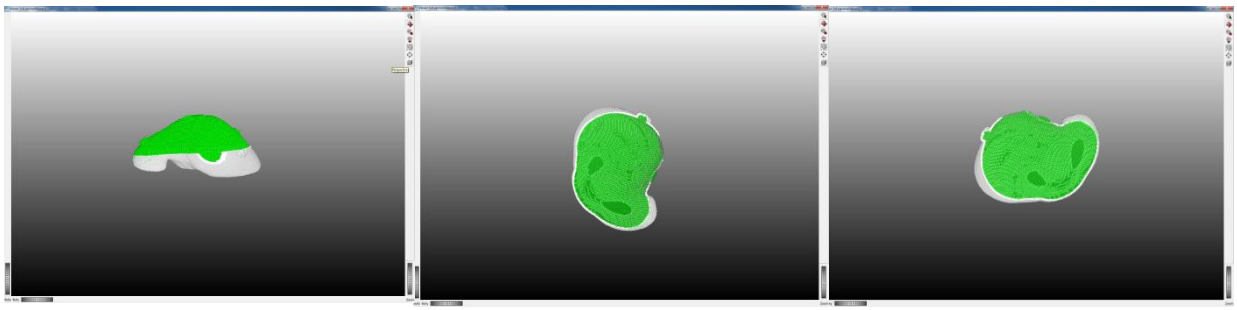

Figure 5.5.2: Left to Right shows the mask fitted to the mesh for fixation of surface vertices of silicon phantom. .

When these boundary conditions are applied to the hierarchical tetrahedral mesh of the MR image of silicon phantom, mesh vertices are basically divided into two parts i.e. the vertices on which displacement fields will be applied and will deform and the vertices for which forces are specified and will not be influenced by application of displacement fields. Because of computationally itensive nature of FEM simualtion procedures, a low resolution mesh was generated. But, for fixation of mesh vertices, there is no need to down sample the fixation mask because it does not interfere with the FEM simulation. If a downsampled mask is used, it would just reduce the number of vertices to be fixated. The mask shown in Figure 5.5.1 fixes 5962 vertices on the surface of volume mesh.

5.6 Visualization

Ability to render deformable objects interactively at a high quality is also an essential part after efficient simulation technique for deformable objects. Due to limited resolution of simulations grids, visualizations obtained from these are far below of what is required in medical applications. For real time deformation simulation in medical application, there is a need of a novel volume rendering technique. A state of art GPU volume rendering technique was developed by Joachim Georgii for deformable tetrahedral meshes to achieve high quality visualizations. CPU simulation engine continuously solves the system of linear equations and displaces the finite element grid and then GPU render engine receives displacements and updates the volume mesh accordingly

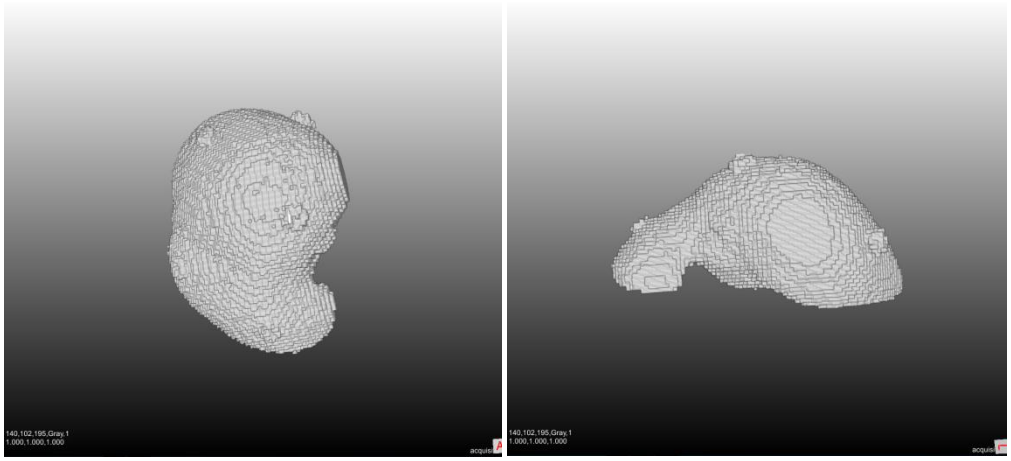

Figure 5.6.1: A voxelized (hierarchical tetrahedral grid) model of the silicon liver phantom used to simulate deformations.

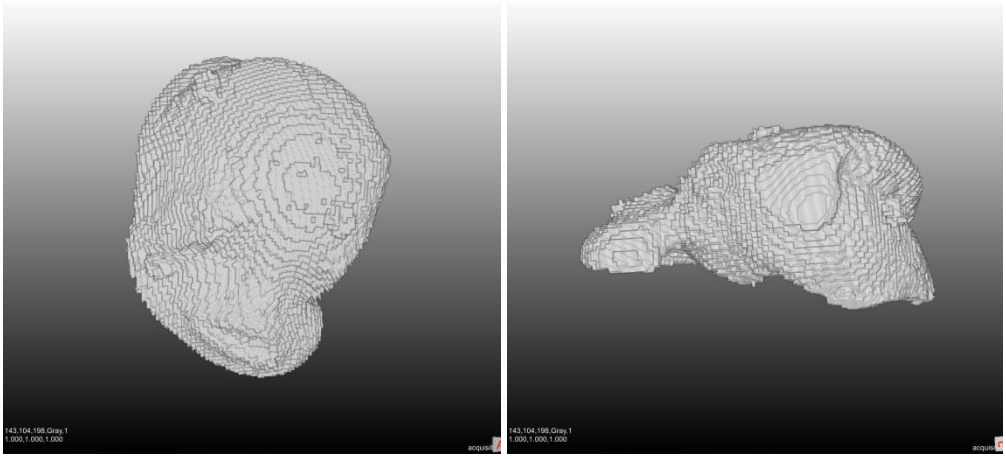

Figure 5.6.2: Deformed voxelized model of silicon liver phantom under specified forces.

Figure 5.6.2 shows the deformed model of silicon phantom. Vertices of the rendered mesh which are fixed by applying boundary conditions are not displaced while, the object as a whole deforms under specified forces. Due to vertex fixation forces, the object is in a deformed state.

A More thorough explanation of rendering of deformable meshes can be found in literature [11]. All the deformation simulations are performed on Intel Core ™ i7 CPU equipped with an NVIDIA GeForce GTS450.

5.7 Generating a simulation model for external forces.

Starting with the initial object representation, a tetrahedral hierarchy that constitutes the basis for multigrid method is generated. Down sampled image used for generation of volume mesh is also used for placement of marker which can be later stretched into a vector across the image. This vector describes the displacement field for FE model and the simulation. A marker can defined anywhere on the 2D image for vector based deformation (see Figure 5.7.1). This marker is then rendered onto the volume mesh. Because, the mesh is generated from a down sampled image, the marker position on an image is rendered as a group of points on the mesh (see Figure 5.7.2). This happens because although the mesh is of low resolution, it has an increased voxel size, which means it covers the same volume as the original data does. This marker can be stretched on the 2D image in arbitrary direction which generates the displacement field from a vector. Thus, external forces are specified and applied at a certain vertices of the mesh. These displacement vectors are then directly added to the global force vector. This global force vector produces the changes in the finite element model and these are given by system of equations. This system of equation is then solved by multigrid solver and these computed displacement updates the geometry of the mesh. Here the interplay between CPU and GPU is effective. While, CPU computes the displacement of objects GPU renders these computed displacements and updates the geometry of the object accordingly. There is a clear separation between the simulation geometry and render geometry which enables the real time deformation simulation based on external forces.

Figure 5.7.1 shows a marker base for a vector on a 2D image and then it is stretched and subsequently Figure 5.7.2 shows the marker base rendered on the volume mesh and then

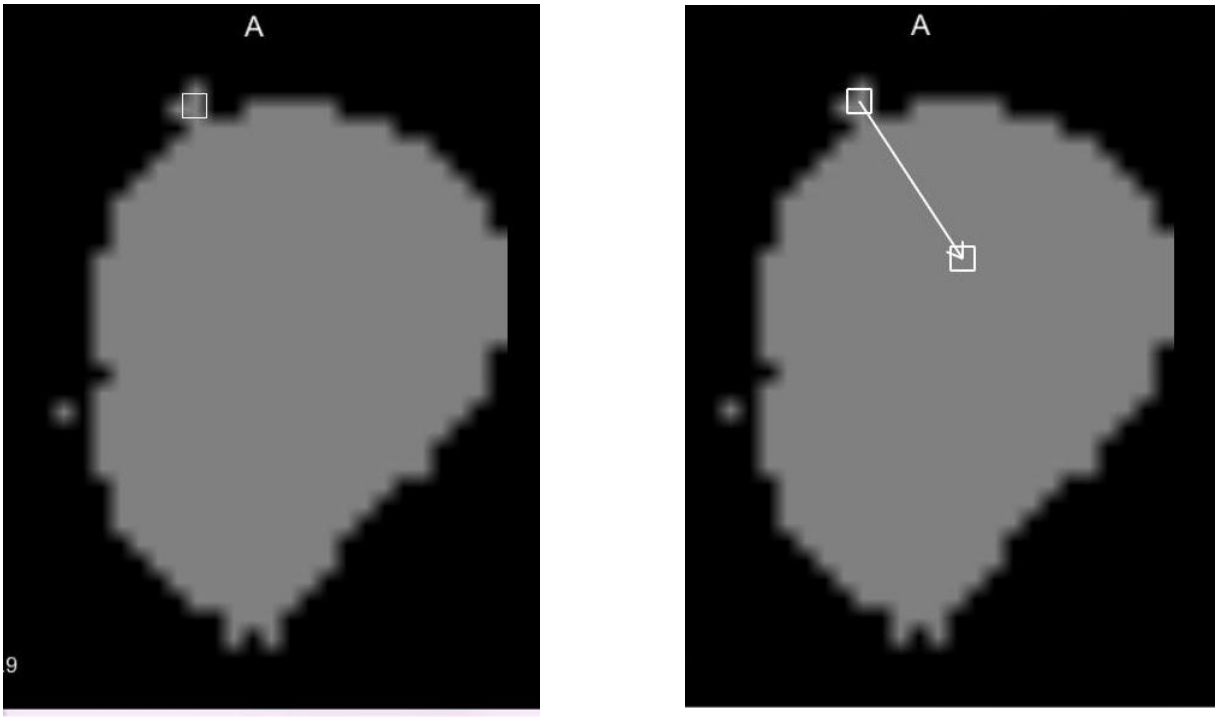

Figure 5.7.1: Left shows 2D down sampled image of silicon phantom with a marker which will then define a vector which will be used for displacement field and right shows a vector which is drawn from the marker base which is then added to global force vector which computes the mesh geometry.

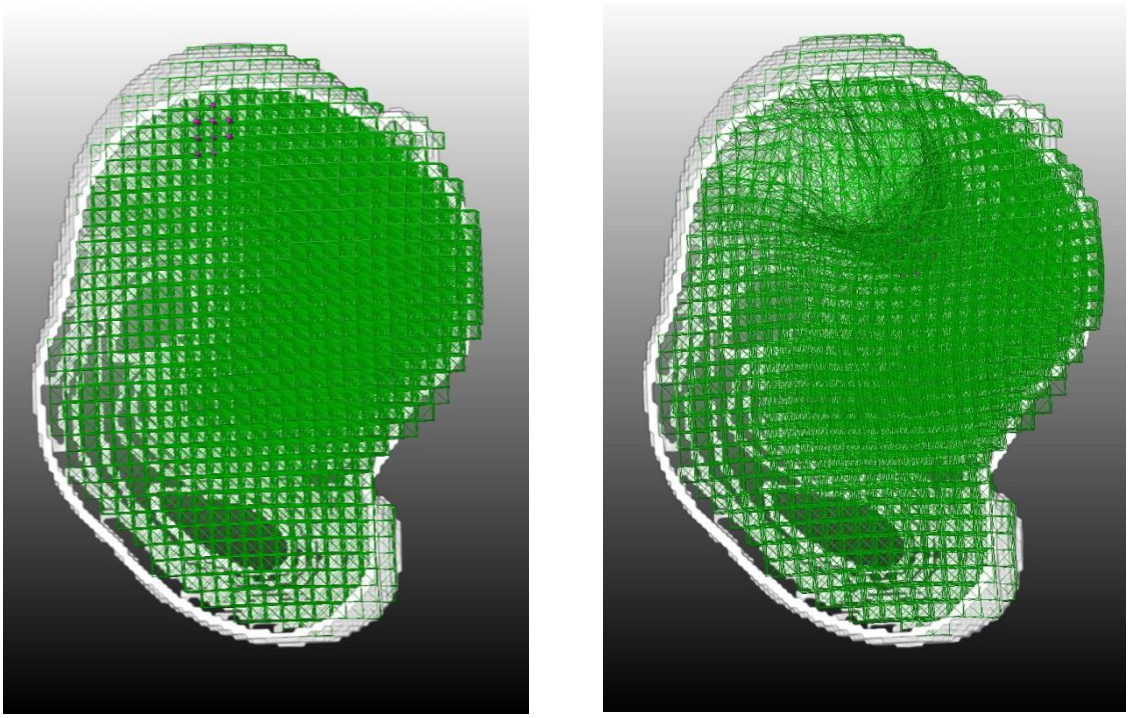

Figure 5.7.2: Left shows a tetrahedral hierarchical mesh whose vertices are fixed which are covered by the mask and the rendered marker shown and right shows an updated geometry of the mesh as per the deformation of finite element model based on the vector defined in Figure 5.7.1

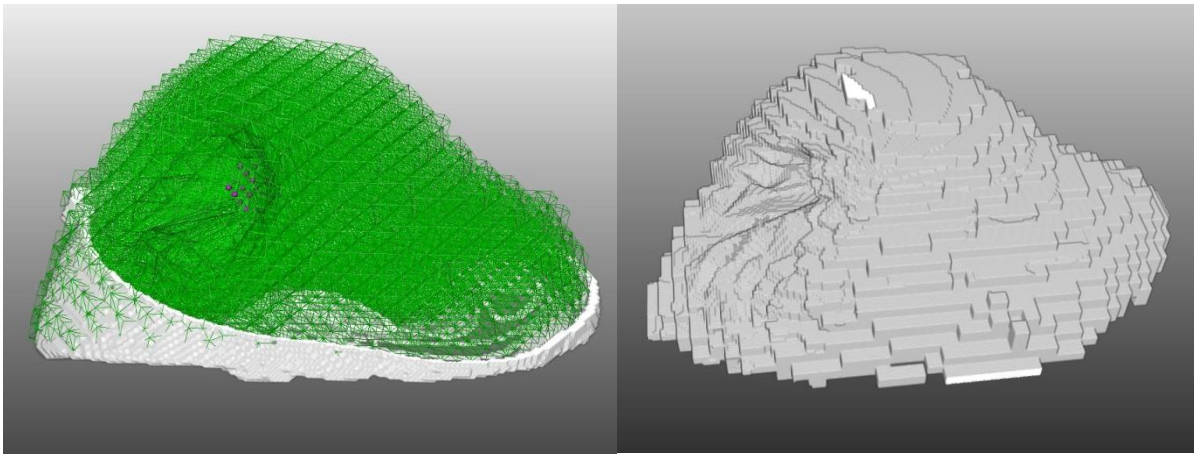

Figure 5.7.3: Left shows an updated geometry of deformed mesh in different view and right shows an updated rendered deformed voxelized silicon phantom based on the displacement vector defined in figure 5.7.2.

To summarize a deformation simulation model generation based on defined vectors is performed in following steps.

1. Construct a 3D hierarchical tetrahedral finite element mesh.

2. Assign material properties such as stiffness, density, Poisson's ratio.

3. Generate a mask for region on the mesh to be fixed.

4. Fix the surface vertices of model where we do not deformation to take place by defining boundary conditions.

5. Render the vertices of the marker.

6. Set the simulation time step.

7. Stretch the vector in arbitrary direction where we want the deformation to take place.

8. Render the deformed mesh.

This concludes generation of a simulation model which can be handle real time deformation based on vectors defined by user. The vectors which were defined on a 2D image for simulation will then be acquired from a sensor attached to ascension tracking device. And this is explained in the next chapter.

6. Non rigid registration

This chapter describes the interplay of two systems described above. First, rigid registration based on mathematical mapping. Second, FEM model used to define deformation simulation from external forces. The combination of these two gives us non-rigid registration frameworks which can adapt to real time deformations performed on the silicon phantom as well as it localizes the phantom. Basically, it means that both translational and rotational movements of the phantom along with the deformation can be adapted into real time and visualized. Here, in this section the external forces are input from ascension sensor device.

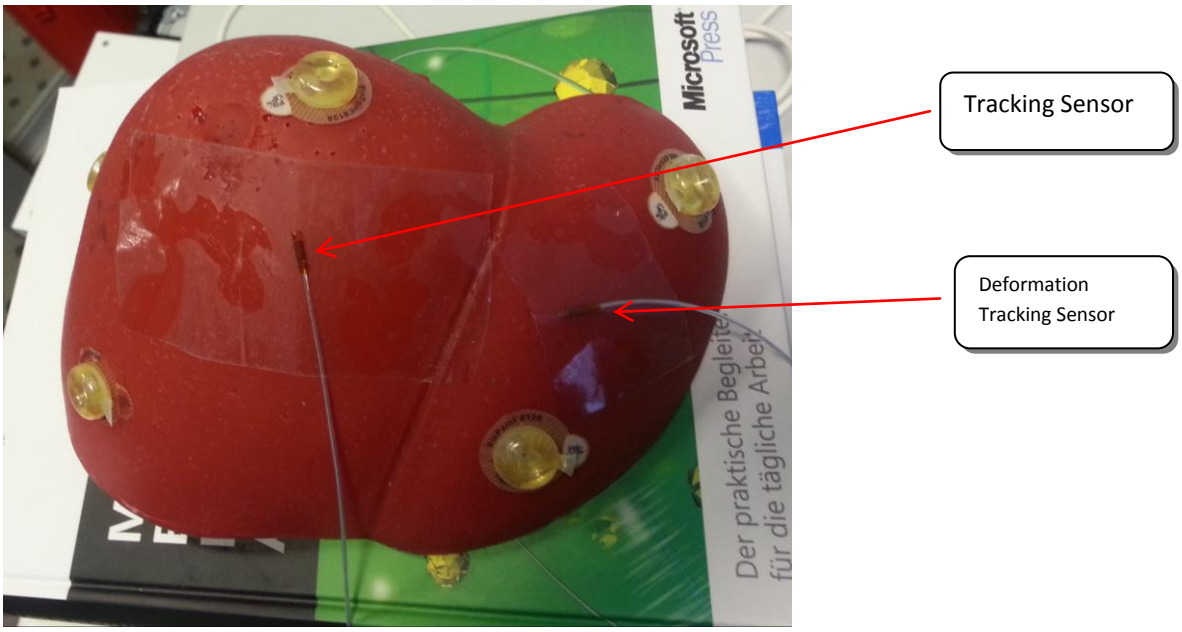

Figure 6.1: Silicon phantom with two attached sensors.

Rigid registration provides with a transformation matrix which maps the coordinates from electromagnetic coordinate system into the image coordinate system. Another sensor (see Figure 6.1) is used for defining displacement vector which can be used for real time simulation. This sensor is then placed on the phantom surface where we want to detect deformation. This sensor is then localized in the image coordinates by

$$\mathbf{T}_{dl} = \mathbf{T} \times T_{ds}$$

Where, T_{ds} is a matrix which provides us with the location of the sensor used for tracking deformation and $\mathbf{T}_{dl}$ is the localized matrix for the deformation sensor. Thus, deformation

sensor is in the image coordinate system and can be applied for visualization (see Figure 6.2). This sensor can be attached anywhere on the surface where deformation has to be tracked. The localized position of the sensor is stored as a marker base and this marker is rendered on the volume mesh of the phantom (see Figure 6.3).

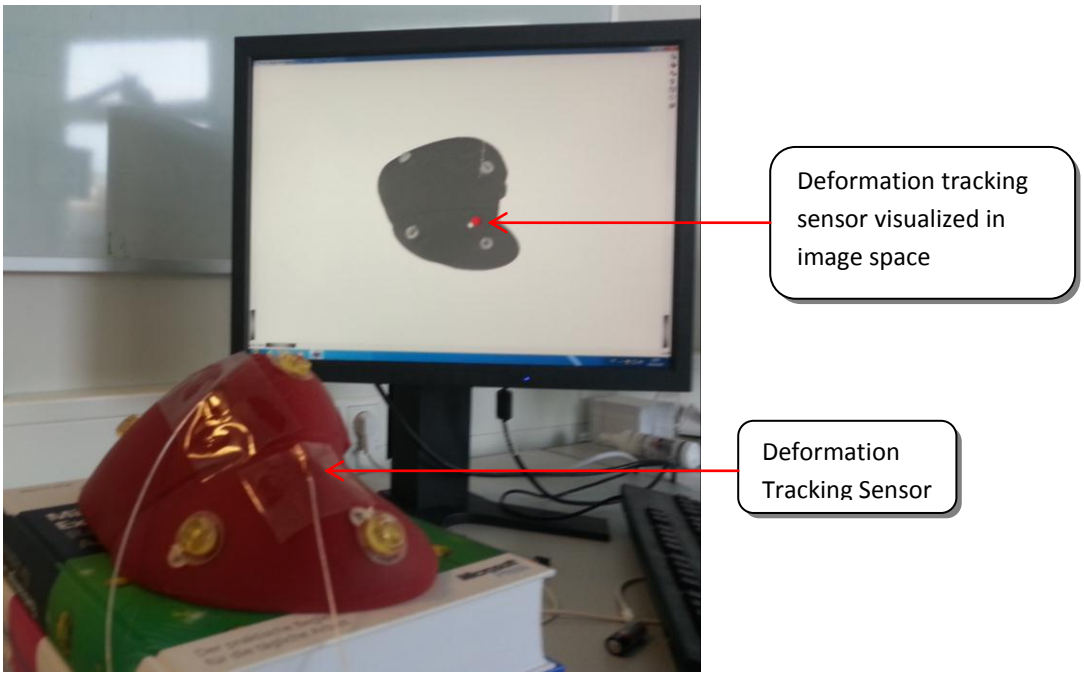

Figure 6.2: Shows the localization of the deformation tracking sensor in image space on the screen

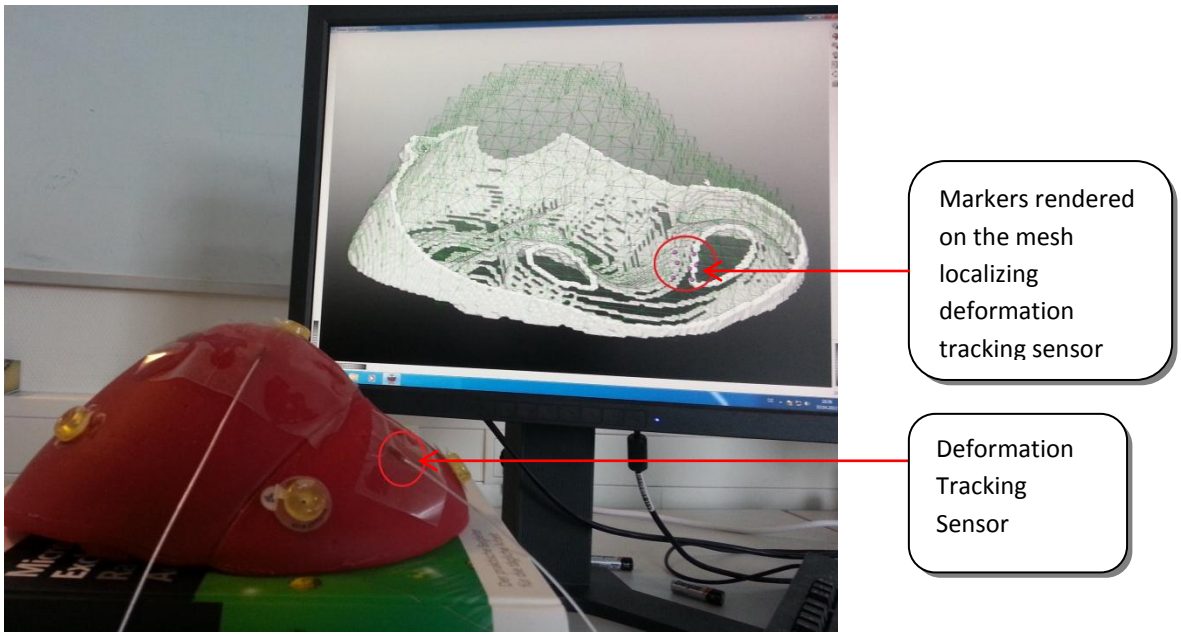

Figure 6.3: Shows the rendering of deformation tracking sensor as a marker on the volume mesh

In order to simulate real time deformations, the sensor is pressed and released. This displacement is recorded as a translational vector from the base position which is updated

continuously as per data received from Ascension™ tracking sensor. This translational vector defines the displacement vector for simulation is similar as shown in Figure 5.7.1. This displacement vector is added to the global force vector, producing changes in the finite element model defined by a system of equations. This system is then solved by a multigrid solver and geometry of the mesh is then updated. Because of rigid registration, this deformation model can still be adapted even if there is any movement of the phantom. The deformed mesh is then rendered as shown in Figure 6.4

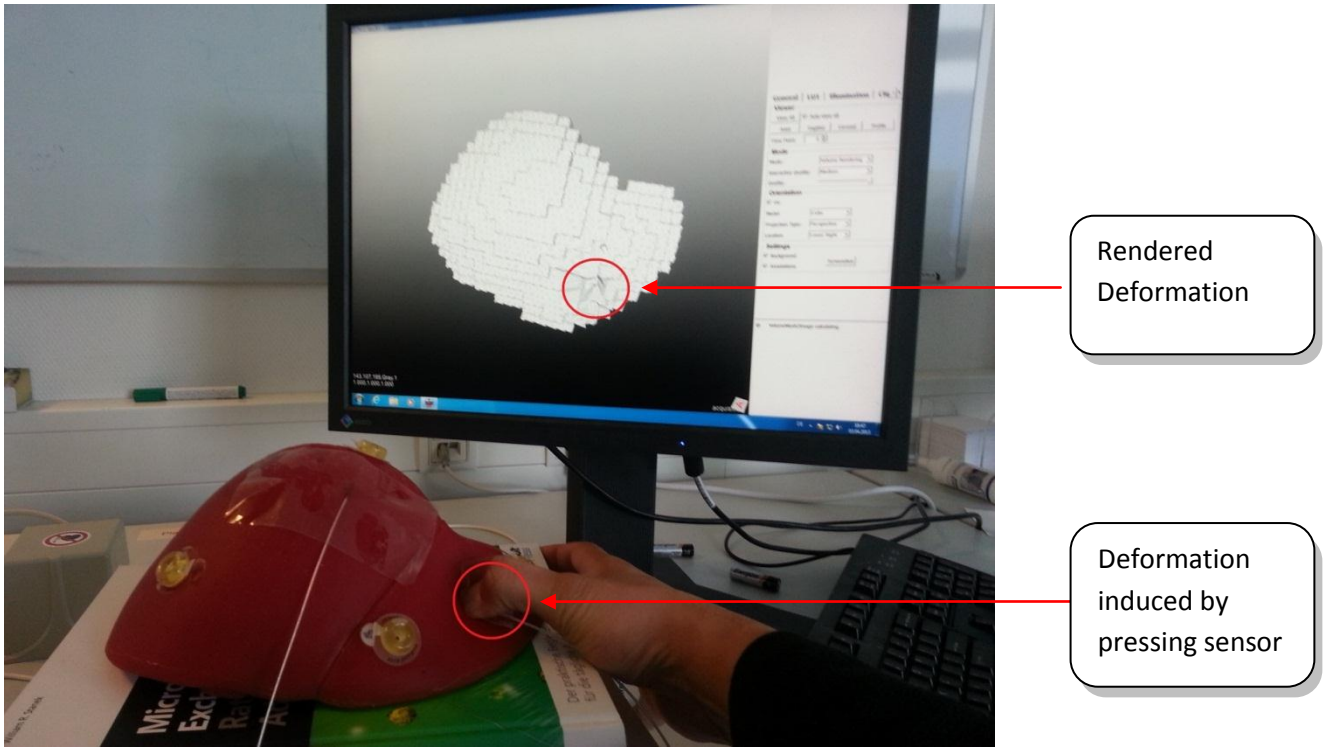

Figure 6.4: Above figure shows the real time deformation simulation based on deformation stimulated by thumb on the silicon phantom where the deformation sensor is attached.

This framework is computationally intensive as there are so many calculations which are to be carried out in real time. Transformation matrix using least square modification of absolute orientation is calculated continuously and based on this, the localization of surgical tool and localization of deformation tracking sensor is also carried out continuously. Also, the deformation vector generated for simulation of finite element model based on the movement of the deformation tracking sensor is also generated continuously. The GPU cannot update high resolution mesh geometry in real time simulation time step. In order to achieve real time deformation simulation we have to compromise on accuracy and precision which is achieved by creating volume mesh from the MR image of silicon phantom is down-sampled to 10% of

its original size using isotropic voxel size. It basically means that the deformations will be performed on much coarser mesh than a finer mesh.

To summarize the entire process (also see Figure 6.5):

1. Initialize Tracking device

2. Capture the location of marker position in correct order

3. Localize these markers based on sensor attached to the phantom surface.

4. Perform registration by mapping markers between acquired positions with corresponding markers in the image

5. Localize the surgical tool

6. Generate Volume Mesh

7. Assign material properties

8. Fix the surface vertices of model where we do not intend to deform

9. Place the sensor tip on the phantom where deformation has to be monitored

10. Localize this position in the image coordinates.

11. Render the vertices of the marker.

6. Set the simulation time step.

7. Deform the liver with help of the sensor.

8. Render the deformed mesh continuously.

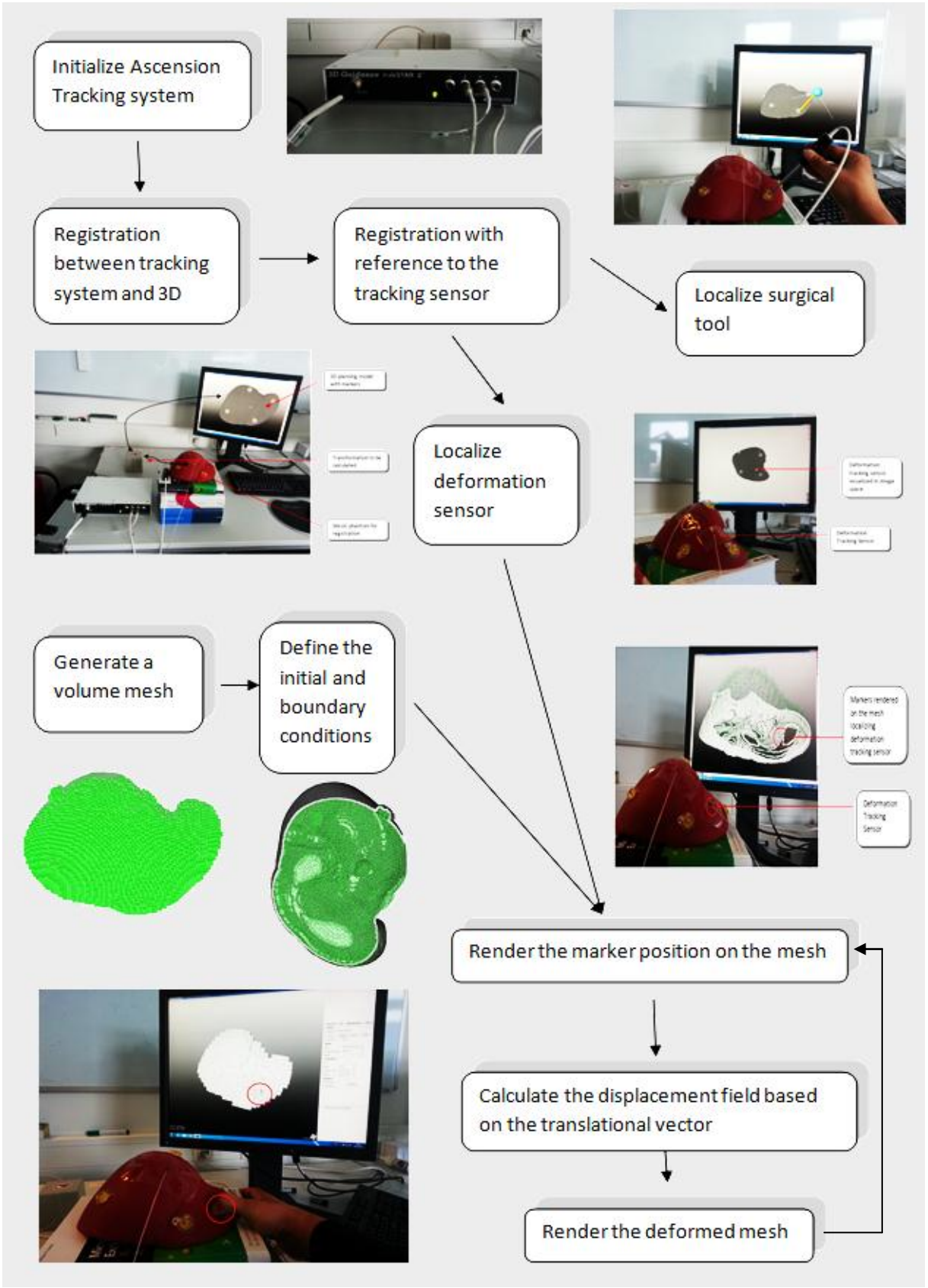

Figure 6.5: Summary of entire process of non-rigid registration with deformation simulation.

This concludes the development of a framework for non-rigid registration.

7. Discussion, Conclusion & Future Aspects

Discussion

The work performed in this thesis utilizing least square parameter estimation for two point patterns for registration mapping between five points on silicon phantom and corresponding five points on the MR image. Section 4.2.2 describes the procedure for finding the transformational parameters (translation, rotation and scaling). Horn presented a closed form method for determination of these parameters, but it failed sometimes to give a correct rotation matrix and instead gave a reflection. Least square estimation theorem in this context always gives a correct transformation matrix even when the data is corrupt [16]. Recent procedures generally use ICP (iterative closest point) algorithm for registration of 3-D shapes. This method handles full six degrees of freedom and always converges monotonically to the nearest local minimum [25]. ICP is useful for matching data sets when the given number of points in each data set is different. However, for same number of coordinates in both data sets, least square estimation gives us a more correct transformation matrix.

In the next Section 4.3 real time registration based on constant update of transformation matrix is explained. Here, the registrations stable even if there is translational and rotational movement of the phantom. Also, in this section localization of surgical instrument is done. This is achieved by simple multiplication of transformation matrix with coordinate matrix of the surgical tool. In this section, silicon phantom, tracking sensor and surgical tool are transformed into image space and everything can be visualized on the screen.

Deformation models are used in wide range of computer graphics applications. Real time application of deformation model is in surgical training and in non-rigid registration for surgical procedures for medical applications [26]. Section 5 describes a deformation simulation model based on implicit finite element modeling. Simulation technique enables realistic and stable simulation of bodies described by tetrahedral grids and corotated Cauchy strain formulation. Section 5.2 describes generation of non-nested hierarchical volume tetrahedral mesh. This is done for appropriate transfer operators to map quantities between different levels of resolutions. The property that a problem can be solved at different levels of resolution can be solved is exploited by the multigrid solver [11] explained in Section 5.4.2.

For the simulation of a physical body it is essential that the material properties such as stiffness, Poisson's ratio and damping factor are assigned which influence the generation of stiffness matrix K by corotated strain formulation defined in Section 5.4.1. Corotated strain is a good trade-off between linear Cauchy strain and non-linear Green strain. Cauchy strain produces artificial forces yielding unwanted results especially when large deformations are applied. Green strain suffers from the disadvantage that it makes the whole system of equations non-linear and thus computationally intensive and difficult to adapt into real time medical applications where accuracy and quick simulation response is required. Corotated formulation splits the motion of every element into rigid body motion with respect to element's initial configuration. Basically, deformed finite elements are first rotated into a configuration that matches the best reference configuration hence, rigid body motions of the element are eliminated before Cauchy strain is computed [19]. Once the rotation of all elements is calculated, stiffness matrix is reassembled. The strain is still approximated linearly, artificial forces which are computed using Cauchy strain is significantly reduced. Dirichlet boundary conditions are defined for vertex fixation. Using this, the system of equations for boundary vertices as well as adjacent vertices is modified. The stiffness matrix is updated as the selective entries are set to zero. For a number of vertices for which displacement is known and the other vertices are fixed by setting their forces to zero, a deformation configuration is obtained that matches the displacement and the other parts of the object are deformed with respect to its physical model [11]. Mass-spring models can also be used for defining a physical model of an object. However, for medical applications the model needs to appear plausible and have visually acceptable results. These conditions are failed to meet by mass spring system models and the application of this model is restricted to Courant condition [11].

Section 6 describes the interplay of rigid registration and deformation simulation model. Here, an extra sensor is attached to the surface which senses the displacement field and adds it to the global force vector which is then used for defining system of equations for finite element model. For adaption of the system into real time application the deformation simulation is applied on a coarser mesh which means that the deformation is not as accurate as intended but, is acceptable for visualization.

For surgical interventions, rigid registration has been extensively studied in the past decades. Rigid registration allows only translation and rotation of the data sets to be registered and

deformations are not considered. Movements due to breathing and motion influenced by surgeon during surgery are not adapted by rigid registration. In rigid registration, pre-operative CT/MR images are mapped with the patient organ. This is commonly known as 3D to 3D image registration which is achieved by least square estimation of transformational parameters between two point patterns developed by Shinji Umeyama. This process of registration is known as point to point registration. Here, anatomical or ficudial markers from the patient are mapped to the corresponding points in the preoperative image. Rigid registration model is not useful when it comes to mapping soft tissues where deformations are also needed to be taken into consideration.

Non-rigid registration has been an area for development and research in recent years. Non-rigid registration techniques also use 3D to 3D point pattern mapping for registration combined with deformation simulation model based on finite element modeling. Real time deformation simulation model used in this thesis was developed by Joachim Georgii. One of the hindrances for non-rigid registration is validation as it is difficult to choose a Gold standard [6]. The FEM simulation model used in this thesis is validated in literature [11].

The field of navigated liver surgery is still evolving and research is now gaining more and more importance. Core components such as tracking systems, registration methods, visualization techniques and simulation models are well established but still continue to evolve [6]. Although clinical systems are developed for surgical procedures, most of these are still in the area of research and development. Only a few are available in market. As surgeries are becoming more and more minimally invasive, navigation and automation are becoming an integral part to improve the quality, precision and accuracy of surgical interventions.

Conclusion

This thesis work describes the experimental development of a non-rigid registration framework. A non-rigid registration framework was successfully constructed and applied for real time tracking of liver motion and deformation using an electromagnetic tracking system. Ascension tracking device used in this thesis is quite precise and does not suffer much from interference. The current registration algorithm used for mapping is pretty stable and can also handle corrupt data and generates fewer errors. The registration framework can handle translational and rotational motions and can also localize surgical instruments. The deformation simulation model is also validated and responds to external forces applied. For real time application, the material properties can be known beforehand and provide more precise and accurate results. Also, this thesis provides a firsthand user experience of corotated Cauchy strain formulation for modeling finite elements which makes the simulation faster and reduces unwanted forces. Dirichlet boundary conditions can be easily applied for surface vertex fixation of a volume mesh. Although these surface vertices which are to be fixed have to defined preoperatively and more work needs to be done if these are to be adapted for real time surgery where the vertices to be fixed can change at any given point. Real time adaption of simulation model is well demonstrated based on displacement vector acquired from external sensor. However, real time adaption suffers from a problem of computational speed and thus it is less precise and deformations induced are less accurate as they are adapted on a coarser tetrahedral mesh. If a faster computer with better GPU is used, finite element model can be solved at a faster rate and GPU can update the mesh geometry at a faster rate we can visualize the updated mesh geometry of a much finer mesh.

Future Aspects

The current version of the framework works efficiently well for real time tracking of liver phantom motion and adapting real time deformation based on finite element modeling. This framework can be further optimized for precise and accurate tracking and modeling of liver phantom. Ascension tracking generator suffers from a problem of orientation. It is necessary that object to be tracked has to be in front also on a level above the generator, otherwise the coordinates localized are not correct. Also, the limited range of 1000mm of the generator can cause a problem if utilized in operating room. Also, non-rigid registration with optical tracking can be an area of extensive research. Ficudial markers can be substituted by optical markers for point patterns matching registration technique. Although deformation simulation based on finite element model is pretty robust, real time adaptation of boundary conditions should be a field to work for actual medical procedures. Deformation based on applied forces can be sensed by using more sensors attached to different lobes of the liver. This framework uses a coarser mesh for performing deformation based on applied external forces which can be made more precise and accurate by using a finer mesh. Also, this framework does not account for cutting performed on the patient's liver. Modeling deformation for simulating cuts can be found in the literature [27]. Also, cutting destroys registration as the object is in parts and the preoperative MR image is not anymore in congruence with the patient's liver. Extensive work can be done in the field of simulating cuts in non-rigid registration by means of finite element modeling.

The current framework can be a platform for further research in the field of non-rigid registration.

Acknowledgement

I would like to thank Dr. Darko Ojdanic for giving me a chance by accepting me as a thesis candidate to elaborate my master thesis at Frauhofer MEVIS, also for his continuous support, guidance and supervision during the thesis.

I would also like to thank Dr. Thomas Schiemann for supervising my thesis and his continuous support throughout the progress of the thesis.

I also thank Dr. Joachim Georgii for allowing me to use his deformation simulation framework for my work.

A special thanks to Dr. Tobias Böhler, Dr. Christian Hansen and Mr. Markus Harz for helpful suggestions during the tenure of my thesis.

I also thank Fraunhofer MEVIS for the software of MeVisLab on which my thesis is based.

Lastly, I would like to thank my family and friends for their support and encouragement which gave me strength to accomplish a difficult task.

Bibliography

[1] "Liver Cancer," [Online]. Available: http://www.cancerresearchuk.org/cancer-info/cancerstats/world/liver-cancer-world/.

[2] M. Peterhans, A. vom Berg, B. Dagon and et.al., "A navigation system for open liver surgery: design, workflow and first clinical applications," vol. 7, no. 1, 2010.

[3] T. Lange, S. Eulenstein, M. Hünerbein and P.-M. Schlag, "Vessel-Based Non-Rigid Registration of MR/CT and 3D Ultrasound for Navigation in Liver Surgery," 2003.

[4] S. Robin, 12 Sep 2011. [Online]. Available: http://www.livestrong.com/article/541792-does-a-pre-op-diet-reduce-a-fatty-liver/. [Accessed 04 03 2013].

[5] D. M. Cash, M. I. Miga, S. C. Glasgow and et.al, "Concepts and Preliminary Data Toward the Realization of Image-guided Liver Surgery," Springer, 2007.

[6] K. Cleary and T. M. Peters, "Image-Guided Interventions: Technology Review and Clinical Applications," Vols. 12:192-142, 2010.

[7] B. Preim and D. Bartz, in *Visualization in Medicine*, Elsevier Inc, 2007.

[8] C. Hansen, "Software Assistance for Preoperative Risk Assessment and Intraoperative Supportin Liver Resection Surgery PhD thesis," 2012.

[9] M. Markert, A. Koschany and T. Lueth, "Tracking of liver for navigation in open surgery," 2009.

[10] W. Lamade and et.al, "Navigation and image-guided HBP surgery: a review and preview," 2002.

[11] J. Georgii, "Real-Time Simulation and Visualization of Deformable Objects-PhD thesis," 2008.

[12] "MeVisLab Features," MeVis Medical Solutions AG, [Online]. Available: http://www.mevislab.de/mevislab/features/. [Accessed 31 01 2013].

[13] "Image Processing," Mevis Medical Solutions AG, [Online]. Available: http://www.mevislab.de/mevislab/features/image-processing. [Accessed 31 January 2013].

[14] "trackSTAR 2," Ascension Technology Corporation, an NDI company, [Online]. Available: http://www.ascension-tech.com/medical/trakSTAR2.php. [Accessed 08 02 2013].

[15] "Ecoflex® Supersoft Silicone," [Online]. Available: http://www.smooth-on.com/Ecoflex%3D-Superso/c1130/index.html. [Accessed 08 02 2013].

[16] S. Umeyama, "Least Squares Estimation of Transformation Parameters between Two Point Patterns," vol. 13, no. 4, 1991.

[17] B. K. P. Horn, "Closed form solution of absolute orientation using unit quaternions," vol. 4, 1987.

[18] L. Chen, "Supporting Navigated Liver Surgery with Pan-Tilt Controller Laser Pointer-Master Thesis," 2011.

[19] J. Georgii and C. Dick, "Efficient Finite Element Methods for Deformable Bodies in Medical Applications".

[20] Á. Alberich-Bayarri and et.al., "Volume Mesh Generation and Finite Element Analysis of Trabecular Bone Magnetic Resonance Images," Lyon, France, 2007.

[21] H. Delingette and N. Ayache, "Soft Tissue Modeling for Surgery Simulation".

[22] J. Georgii and R. Westermann, "A Multigrid Framework for Real-Time Simulation of Deformable Volumes," The Eurographics Association, 2005.

[23] K.-J. Bathe, Finite Element Procedures, 2002.

[24] E. Sifakis and et.al, "Hybrid Simulation of Deformable Solids," Eurographics, 2007.

[25] P. J. Besl and N. D. Mckay, "A Method for Registration of 3-D Shapes," IEEE, 1992.

[26] M. Mueller and et.al, "Real Time Simulation of Deformation and Fracture of Stiff Materials".

[27] C. Dick, J. Georgii and R. Westermann, "A Hexahedral Multigrid Approach for Simulating Cuts in Deformable Objects," IEEE TRANSACTIONS ON VISUALIZATION AND COMPUTER GRAPHICS, 2010.